Distinct spatiotemporal dynamics of CD8+T cell-derived cytokines in the tumor microenvironment

Hoekstra, M.E.; Slagter, M.; Urbanus, J.; Toebes, M.; Slingerland, N.; Rink, I. de; ... ; Schumacher, T.N.

Cancer Cell

Report

Distinct spatiotemporal dynamics of CD8$^+$ T cell-derived cytokines in the tumor microenvironment

Graphical abstract

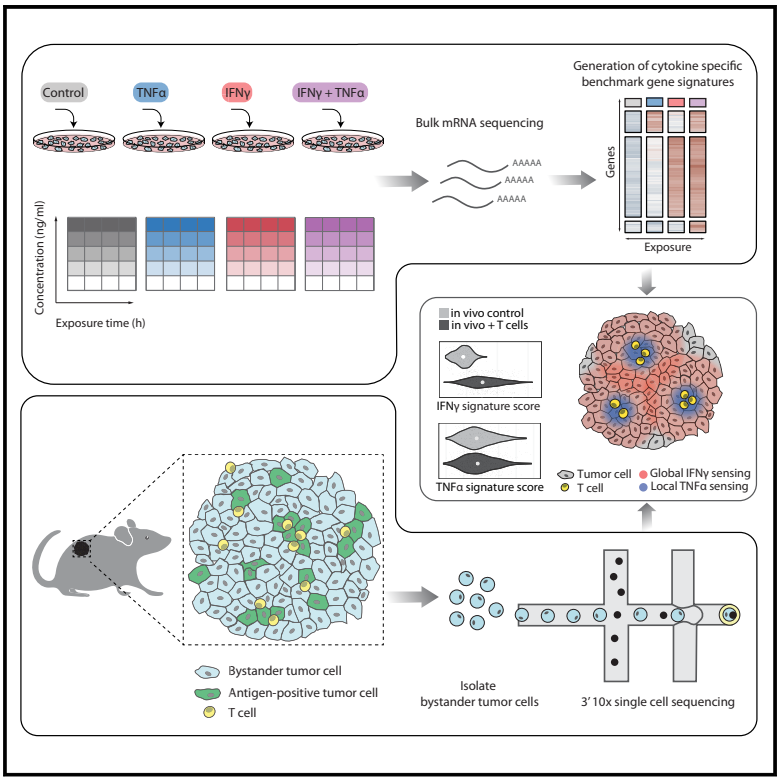

Authors

Mirjam E. Hoekstra, Maarten Slagter, Jos Urbanus, ..., Ron Kerkhoven, Lodewyk F.A. Wessels, Ton N. Schumacher

Correspondence

t.schumacher@nki.nl

In brief

Hoekstra et al. describe a single-cell RNA-seq-based approach for inference of prior *in vivo* cytokine sensing. They demonstrate that CD8$^+$ T cell-derived TNFα is only sensed locally in the TME, whereas IFNγ forms a global tumor tissue modifier, and such IFNγ sensing appears associated with suppressed TGFβ sensing.

Highlights

- Single cell transcriptomes inform on prior cytokine sensing
- CD8$^+$ T cell-derived interferon γ (IFNγ) is a dominant modifier of the tumor microenvironment (TME) as compared to tumor necrosis factor α (TNFα)
- TGFβ sensing appears lowered in IFNγ sensing tumor cells
- Cytokines may be distinguished into local and global tissue modifiers

Hoekstra et al., 2024, Cancer Cell *42*, 157–167
January 8, 2024
https://doi.org/10.1016/j.ccell.2023.12.010

CellPress

Cancer Cell

CellPress
OPEN ACCESS

Report

Distinct spatiotemporal dynamics of CD8$^+$ T cell-derived cytokines in the tumor microenvironment

Mirjam E. Hoekstra,[1,6,8] Maarten Slagter,[1,3,7,8] Jos Urbanus,[1] Mireille Toebes,[1] Nadine Slingerland,[1] Iris de Rink,[2] Roelof J.C. Kluin,[2] Marja Nieuwland,[2] Ron Kerkhoven,[2] Lodewyk F.A. Wessels,[3,4] and Ton N. Schumacher[1,5,9,*]

[1]Division of Molecular Oncology & Immunology, Oncode Institute, The Netherlands Cancer Institute, Amsterdam, the Netherlands
[2]Genomics Core Facility, The Netherlands Cancer Institute, Amsterdam, the Netherlands
[3]Division of Molecular Carcinogenesis, Oncode Institute, The Netherlands Cancer Institute, Amsterdam, the Netherlands
[4]Department of EEMCS, Delft University of Technology, Delft, the Netherlands
[5]Department of Hematology, Leiden University Medical Center, Leiden, the Netherlands
[6]Present address: Division of Molecular Pathology, Oncode Institute, the Netherlands Cancer Institute, Amsterdam, the Netherlands
[7]Present address: CureVac Netherlands B.V., Amsterdam, the Netherlands
[8]These authors contributed equally
[9]Lead contact
*Correspondence: t.schumacher@nki.nl
https://doi.org/10.1016/j.ccell.2023.12.010

SUMMARY

Cells in the tumor microenvironment (TME) influence each other through secretion and sensing of soluble mediators, such as cytokines and chemokines. While signaling of interferon γ (IFNγ) and tumor necrosis factor α (TNFα) is integral to anti-tumor immune responses, our understanding of the spatiotemporal behavior of these cytokines is limited. Here, we describe a single cell transcriptome-based approach to infer which signal(s) an individual cell has received. We demonstrate that, contrary to expectations, CD8$^+$ T cell-derived IFNγ is the dominant modifier of the TME relative to TNFα. Furthermore, we demonstrate that cell pools that show abundant IFNγ sensing are characterized by decreased expression of transforming growth factor β (TGFβ)-induced genes, consistent with IFNγ-mediated TME remodeling. Collectively, these data provide evidence that CD8$^+$ T cell-secreted cytokines should be categorized into local and global tissue modifiers, and describe a broadly applicable approach to dissect cytokine and chemokine modulation of the TME.

INTRODUCTION

Tumors are composed of a diversity of interacting cell types, including tumor cells, fibroblasts, endothelial cells, and a variety of immune cell types. A first type of interactions between the cell populations that jointly form the tumor microenvironment (TME) is formed by direct cell-cell contacts, and to describe the effects of such cellular interactions, technologies such as PIC-seq, which allows mRNA-sequencing of physically interacting cell pairs, have been developed.[1] Importantly, next to such direct cell-cell interactions, cells also use soluble factors, such as cytokines, chemokines, and growth factors, to influence the state of surrounding tissue cells.[2]

One of the major cytokine-producing cell compartments in tumor tissue is formed by the CD8$^+$ cytotoxic T cell pool, and CD8$^+$ T cells have been demonstrated to play a central role in both immune checkpoint blockade[3] and adoptive T cell therapies.[4–6] Upon encounter of antigen-expressing target cells, CD8$^+$ T cells release lytic granules containing cytotoxic molecules such as perforin and granzymes in the synapse that is formed between the interacting cells. In addition, T cell receptor (TCR) signaling leads to the secretion of the cytokines interferon γ (IFNγ), tumor necrosis factor α (TNFα) and interleukin-2 (IL-2), which can, on their own or jointly, induce large-scale alterations in the transcriptome of cells that sense these factors. For example, IFNγ receptor (IFNγR) signaling has been demonstrated to result in increased expression of components of the antigen presentation pathway, enhances expression of immune checkpoint molecules, and can promote recruitment of other immune cells through production of chemokines such as CXCL9, 10 and 11.[7,8] In addition, IFNγ and TNFα have been demonstrated to regulate the activation and maturation state of, among others, macrophages and dendritic cells.[9–12] Furthermore, both IFNγR and TNFα receptor (TNFαR) signaling can, in a context-dependent fashion, contribute to tumor cell senescence,[13] apoptosis[8,14] and ferroptosis.[15] Finally, besides their direct effects on tumor cells, both IFNγ and TNFα can also be critical for tumor control through their effects on stromal cells in the tumor vasculature.[16–20]

In spite of the central role of T cell-produced cytokines in the modulation of cell behavior in the TME, our understanding of the spatiotemporal behavior of CD8$^+$ T cell derived cytokines is

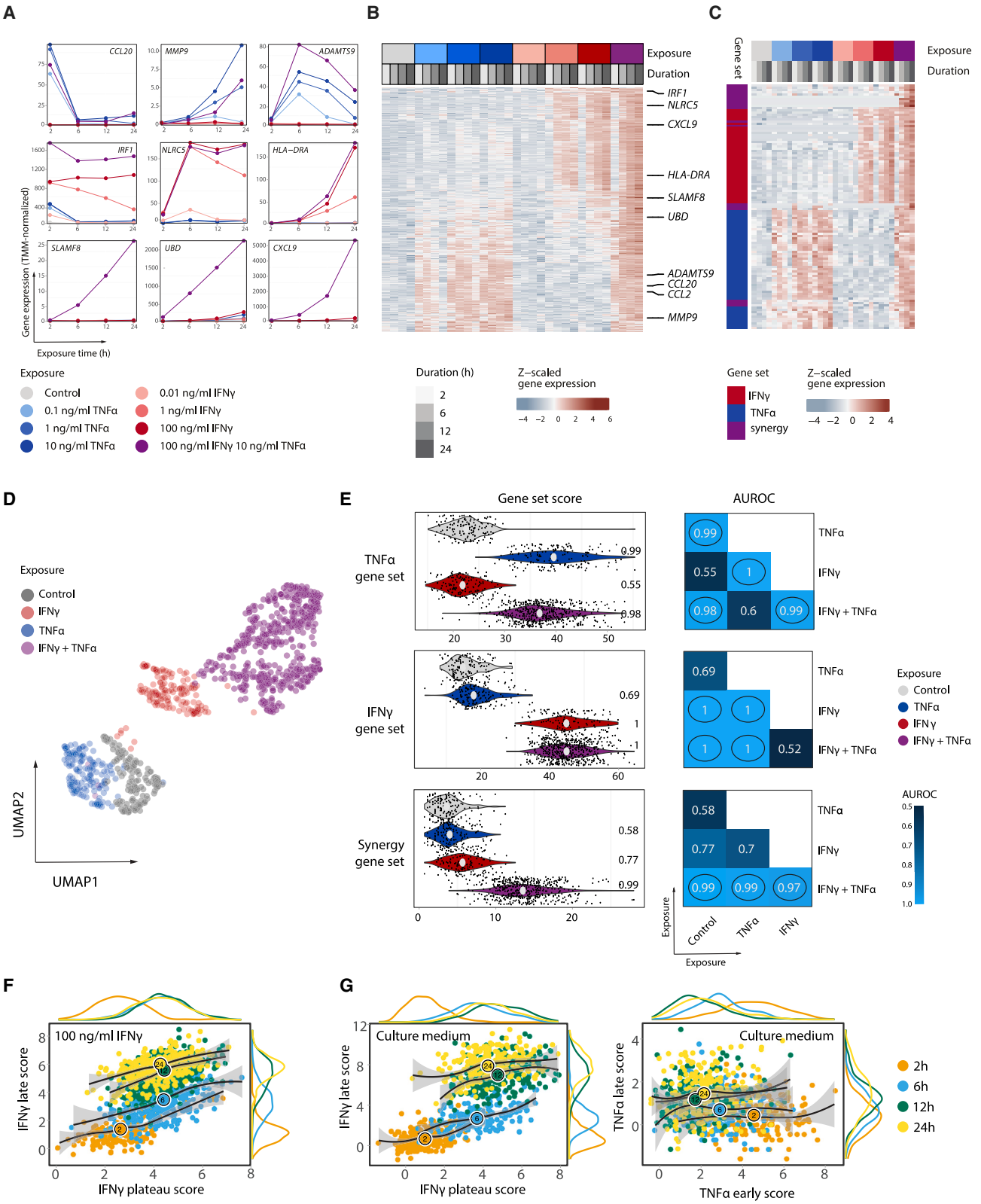

Figure 1. Gene expression informs on cytokine exposure

(A) mRNA expression profiles of selected genes in OVCAR5 cells exposed to indicated concentrations of IFNγ, TNFα, or their combination, for the indicated duration. Top, middle, and bottom panels depict genes that are primarily responsive to TNFα, IFNγ, or TNFα *plus* IFNγ, respectively.

(legend continued on next page)

limited. Specifically, it has not been established whether these signaling molecules differ in their capacity to not only influence target cells in the immediate vicinity of sites of antigen recognition, but also modulate the behavior of cells in the tumor tissue in a more global manner. Earlier work has demonstrated that cytokines may either be secreted in a multidirectional fashion, or can selectively be released in the immune synapse, analogous to the focused release of lytic granules.[21] Specifically, following TCR triggering, membrane-bound TNFα has been shown to be distributed equally over the cell membrane, as demonstrated by live imaging of TNFα on activated murine CD4$^+$ T cells.[21] In contrast, in clusters of T cells and antigen-presenting cells, IFNγ, IL-2, IL-4, and IL-5 were all shown to be localized at the microtubule organizing center (MTOC), consistent with directional release.[21–23] Based on this postulated difference in mode of secretion, a more profound effect of TNFα relative to, for instance, IFNγ or IL-2 on cells that are distant from the site of antigen recognition could be expected. However, as the size of the cell field in which productive cytokine sensing can occur is also influenced by other parameters, such as cytokine half-life, receptor-mediated clearance, and binding to extracellular components, it has been difficult to predict the extent of long range sensing of different cytokines in the TME.[24]

Evidence that cytokines can reach (remote) bystander cells that cannot be recognized by T cells directly has been obtained in a number of studies in both viral infection and tumor models.[25–30] Specifically, T cell-secreted IFNγ in skin and lymph nodes was shown to induce expression of IFNγ-responsive genes in large regions outside the parasite or virus infected areas.[26,27,31] Likewise, secretion of IFNγ and TNFα by CD4$^+$ T cells in tumors has been demonstrated to induce senescence in tumor cells that cannot be directly recognized by T cells.[13] In case of CD8$^+$ T cells, long-range sensing of IFNγ has been observed by, among other, intravital imaging of fluorescent IFNγR-signaling reporters in mosaic tumors that contain both antigen-positive and antigen-negative tumor areas. Using such fluorescent reporter systems, it was demonstrated that a large fraction of bystander cells senses IFNγ upon intratumoral T cell activation, and that IFNγ sensing can occur in tumor cells at distances over hundreds of micrometers from the site of T cell activation.[29,30] Collectively, these data on individual cytokines provide an incentive to develop technology to measure and deconvolute the joint effects of multiple cytokines on the TME.

In the present study, we set out to generate a strategy that allows the analysis of the effects of a broad set of cytokines simultaneously, and also provides information on the timing of such cytokine exposure. The data obtained demonstrate that, contrary to what would be predicted based on their mode of secretion, IFNγ is the dominant T cell-secreted modifier of the TME.

RESULTS

Gene expression informs on prior cytokine sensing

In order to measure cytokine sensing in the TME in a manner that is independent of genetic reporter systems, we explored whether gene expression signatures can reliably inform on the type and duration of cytokine exposure. Toward this goal, we exposed human ovarian carcinoma (OVCAR5) cells to different cytokines or cytokine combinations for 2–24 h and analyzed transcriptomes by bulk mRNA sequencing (RNA-seq). In line with expectations, this revealed large groups of genes that were selectively induced by IFNγ (such as *HLA-DRA* and *IRF1*), or TNFα (such as *CCL20* and *MMP9*). In addition, a gene set was identified that was either preferentially or exclusively induced by the combination of these cytokines (e.g., *UBD* and *CXCL9*) (Figure 1A). Furthermore, the relative expression of individual genes in these gene sets provided rich information on cytokine exposure time, distinguishing genes with a "burst-like" expression pattern (e.g., *CCL20* after TNFα exposure), and genes for which expression showed an exponential increase over time (e.g., *MMP9* after TNFα exposure) (Figure 1A). While gene expression data were rich in terms of the nature and duration of cytokine exposure (Figures 1A and 1B), no substantial differences in gene expression were observed as a function of cytokine concentration beyond a limited concentration range (∼10-fold range). Importantly, cell culture medium derived from T cell-tumor cell co-cultures contained high levels of IFNγ (>100 ng/mL) and TNFα (±1 ng/mL) and induced a gene expression profile that was highly similar to that observed upon dual IFNγ *plus* TNFα exposure (Figure S1A).

To be able to assign duration and type of cytokine exposure to individual cells, we compiled a set of cytokine informative genes through a combination of model training and manual curation. In brief, to efficiently expand a seed set of ∼80 informative genes identified by manual selection, all genes were annotated with descriptive features (see STAR methods), developed to discern

(B) Heatmap of bulk gene expression values inferred from OVCAR5 cells exposed to indicated concentrations of TNFα, IFNγ, or TNFα *plus* IFNγ, for indicated durations. Unsupervised hierarchical clustering of data (shown are the 612 genes from the "cytokine-responsive class"), groups samples by exposure type and then by exposure duration.

(C) Heatmap of bulk gene-expression values for mono-responsive genes and synergy genes inferred from *in vitro* stimulated OVCAR5 cells, as in (A) and (B). Unsupervised hierarchical clustering of gene expression data shows a nearly full agreement with assigned gene classes (cluster purity of 0.86).

(D) UMAP of scRNA-seq data of OVCAR5 cells stimulated with indicated recombinant cytokines for 24 h.

(E) Gene set scores for scRNA-seq data of *in vitro* cytokine stimulated cells as in a. Left panels: dots represent gene set scores of individual cells violins represent densities of score distributions, white dots represent group medians. Area under the receiver operator curve (AUROC) values, quantifying how well experimental conditions can be distinguished from the control condition, are depicted. Right panels: Heatmaps showing pairwise distinguishability of indicated experimental conditions (axes) using gene set scores, as quantified using AUROC values. Comparisons for which indicated gene sets are designed to show separation are encircled.

(F) IFNγ plateau versus IFNγ late gene set scores (see STAR methods) for OVCAR5 cells stimulated with IFNγ (100 ng/ml) for the indicated times. Black lines are LOESS-smoothed curves representing local averages, one per stimulus duration. The ratio of each of the two gene set scores informs on duration of cytokine exposure.

(G) IFNγ plateau versus IFNγ late gene set scores and TNFα early versus TNFα late gene set scores for OVCAR5 cells stimulated with culture medium obtained from T cell-tumor cell co-cultures for the indicated times as in (F). See also Figures S1, S2, and Table S1.

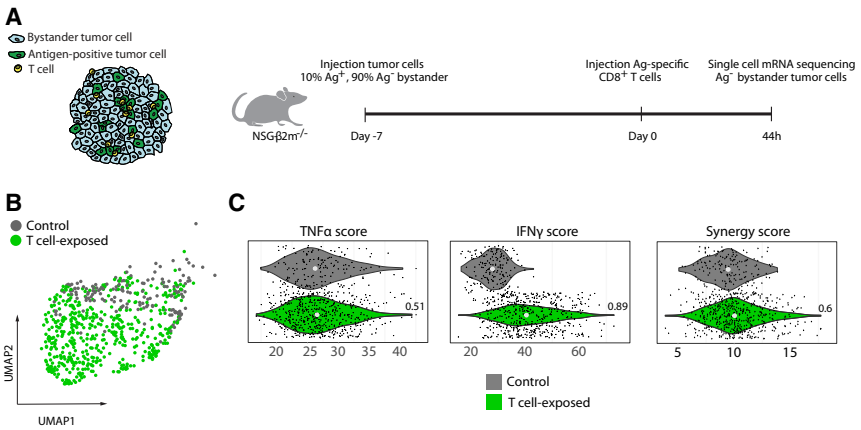

Figure 2. Frequent IFNγ but not TNFα sensing by bystander tumor cells

(A) NSG-β2m$^{-/-}$ mice injected subcutaneously with a mixture of 10% CDK4$_{R>L}$ antigen expressing and 90% bystander OVCAR5 tumor cells were treated with either PBS (control) or CDK4$_{R>L}$-specific CD8$^+$ T cells after tumor establishment. Tumors were harvested 44 h after treatment, and bystander tumor cells were analyzed by scRNA-seq.

(B) UMAP of single cells based on gene expression in the "cytokine-responsive" gene class.

(C) TNFα, IFNγ, and synergy gene set scores of single cells derived from OVCAR5 tumors. Dots represent gene set scores of individual cells, violins represent densities of score distributions, white dots represent group medians. Numeric values reflect AUROC values that quantify separability between experimental conditions. Note that IFNγ, but not TNFα, gene set scores are increased in the T cell-exposed condition as compared to the control condition. See also Figure S3.

cytokine-responsive from unresponsive genes (Figure S1B). We next iteratively expanded from this initial seed set by training a machine learning model with the objective of predicting gene classes (e.g., "cytokine-responsive" and "cytokine-unresponsive") for all yet unclassified genes (Figures S1C and S1D). After 10 iterations of model training, gene class prediction, and correction of predicted classes, a set of 612 cytokine-responsive genes was obtained. (Figure S1E). 90 of these could be classified as mono-responsive to either IFNγ (n = 40) or TNFα (n = 50), i.e., with only a single cytokine eliciting a response and IFNγ *plus* TNFα eliciting a response that did not substantially deviate from the response to the main excitatory cytokine. This property renders these genes especially useful when simultaneously assessing the spreading behavior of both cytokines (Figures S1F and 1C) and allows for the summing of expression values for component genes to infer cytokine stimulus (see the following text). Importantly, comparison of these gene sets to the TNFα and IFNγ Hallmark gene sets[32] that are frequently used to evaluate signaling revealed only modest overlap (Figure S2A). Whereas the newly developed gene sets consisted solely of genes that responded strongly and specifically to the cytokine they were assigned to in OVCAR5 cells, the Hallmark gene sets showed considerable overlap. Furthermore, a sizable number of TNFα hallmark genes was shown to respond to IFNγ and vice versa, creating the potential for incorrect signal inference (Figures S2B–S2D). Next to the set of mono-responsive genes, a set of synergy genes, which are selectively expressed in the presence of both IFNγ and TNFα, was identified, providing an independent means to measure co-occurrence of IFNγR and TNFαR signaling (Figure 1C). Finally, analysis of gene expression dynamics demonstrated that this approach can inform on cytokine exposure duration (Figure S2E).

Frequent IFNγ but not TNFα sensing by bystander tumor cells in the TME

Having established a number of cytokine- and time-informative gene sets, we tested whether gene expression upon cytokine exposure is informative in single cell (sc) transcriptome data. In an unsupervised analysis, cells exposed to activating concentrations of either IFNγ, TNFα, or their combination formed separated clusters, both from control cells and each other, (100% rejection rate on kBET-test[33] with stimuli as batches; median silhouette width: 0.17) (Figure 1D). To quantify signal strength for each exposure-specific gene set, we subsequently calculated cell expression scores for all genes that were included in either gene set. Using this strategy on scRNA-seq data from cells exposed to activating concentrations of IFNγ or IFNα revealed a near perfect separation of IFNγ and TNFα exposed cells from control cells, as well as a clear separation between cells exposed to the two different stimuli (Figure 1E). In addition, exposure to the combination of IFNγ *plus* TNFα could be identified with high precision, both by analysis of the separate IFNγ and TNFα gene set scores, and by use of the IFNγ *plus* TNFα synergy gene set (Figure 1E). Furthermore, ability to correctly assign cytokine stimuli was not affected by the experimental strategy (protease digestion, flow cytometric sorting) required to obtain single cell information from tumor material (Figure S2F). Finally, use of time-informative gene sets on *in vitro* cultured cells exposed to recombinant cytokines or culture medium from T cell-tumor cell co-cultures at different time points demonstrated the ability of this technique to also infer stimulus duration from single cell data (Figures 1F, 1G, and Table S1).

Having established methodology for TNFα and IFNγ exposure inference in single cells, we subsequently set out to measure the degree of T cell-secreted cytokine sensing by tumor cells in the TME *in vivo*. To this purpose, OVCAR5 tumors that were composed of a large fraction of antigen negative ("bystander") tumor cells that could serve as cytokine sensing reporter cells, plus a small fraction of tumor cells that form targets for neoantigen-specific T cells[30] were established in NSG-β2m$^{-/-}$ mice (Figure 2A). Following treatment of mice bearing such mosaic tumors with TCR-transduced CDK4$_{R>L}$ neoantigen-specific CD8$^+$ T cells, infiltration of CD8$^+$ T cells into tumor tissue is observed and upon target cell recognition, cytokine production is initiated in tumor regions composed of antigen-positive tumor cells.[30] Note that in this setup, all subsequent analyses of cytokine-specific gene set scores by scRNA-seq were restricted to antigen negative bystander cells that cannot be recognized by T cells, and hence were not influenced by direct cell-to-cell killing of antigen-positive tumor cells.

Having established that T cell infiltration and activity are first detected around 16 h and increase up to 44 h after T cell transfer

(Figure S3A), we analyzed bystander tumor cells by scRNA-seq at 16–44 h after T cell transfer. Unsupervised clustering of bystander cells derived from 44 h T cell-exposed tumors and control tumors demonstrated a separation of a large fraction of bystander cells obtained from T cell-exposed tumors (Figure 2B). Thus, the presence of a tumor-reactive $CD8^+$ T cell compartment substantially modifies the transcriptome of a considerable part of bystander tumor cells in the TME. Importantly, assignment of cells to different cytokine exposure conditions revealed that a large fraction (70.4%) of bystander tumor cells in T cell-treated mice showed a pronounced IFNγ gene set score, whereas such IFNγ sensing was largely absent in tumor cells from control mice (5.3% of cells) (Figures 2C and S3B). In contrast, presence of a tumor-reactive T cell compartment did not measurably increase the fraction of TNFα sensing cells, with 5.3% of tumor cells classified as TNFα sensing in both control and T cell-exposed tumors (Figures 2C and S3B). In addition, tumor cells displaying high IFNγ gene set scores did not show elevated TNFα gene set scores (Figure S3B). As a second test of *in vivo* TNFα exposure, we calculated synergy gene set scores, which independently inform on the sensing of the combination of IFNγ *plus* TNFα (Figures 2C and S3B). Also by this metric, the presence of a tumor-reactive T cell compartment did not result in TNFα sensing by an appreciable fraction of bystander tumor cells. As a majority of TNFα genes displays a burst-like, early, expression pattern, we next assessed cytokine sensing at the 16 h timepoint, at which measurable T cell infiltration is just visible (Figure 3A). Already at this time point, a subset of bystander tumor cells derived from T cell-exposed tumors separated from bystander tumor cells in control tumors (Figure 3B). However, neither the use of the entire TNFα mono reporter gene set (Figure 3C, left), nor the use of the TNFα early time-informative gene set, showed an appreciable TNFα sensing signal (Figure 3D, right). Note that T cells derived from such tumors did retain the capacity to produce TNFα, indicating that the lack of an appreciable tumor cell population that showed TNFα sensing was not explained by impaired cytokine production (Figure S3C). As a side note, application of the time reporting IFNγ-responsive gene sets demonstrated that tumor cells isolated 44 h after T cell infusion that show a given expression of the IFNγ "plateau gene set score" on average showed a slightly increased expression of the IFNγ "late gene set score," as compared to tumor cells analyzed 16 h after T cell infusion (Figure 3D, left). To test whether bystander tumor cells did retain the capacity to respond to TNFα *in vivo* when this cytokine is present, we intratumorally injected tumors with recombinant cytokines. Importantly, an evident TNFα signal was observed upon injection of either TNFα (with 53.4% of cells surpassing 95th percentile of control) or TNFα *plus* IFNγ (51.8%) (Figures 3E and S3D), Furthermore, a pronounced synergy signal was selectively observed upon intratumoral injection of TNFα *plus* IFNγ (49.4% of cells), likewise indicating a high sensitivity to detect TNFαR signaling *in vivo*.

To test whether the observed difference in long-range IFNγ and TNFα sensing also occurs in syngeneic tumor models, in which not only tumor cells but also infiltrating immune cells can respond to T cell-secreted cytokines,[34,35] we compiled responsive gene sets from cytokine-stimulated mouse NRAS mutant melanoma (NMM) cells (Figure S4A). Application of these gene sets to bystander cells derived from mosaic NMM tumors demonstrated that a large fraction of bystander tumor cells (38.0%) responded to IFNγ in T cell-treated mice, as compared to bystander tumor cells in mice that did not receive antigen-specific T cells (5.1%), or in mice in which antigen was lacking (5.7%). In contrast, presence of a tumor-reactive $CD8^+$ T cell compartment did not induce sensing of TNFα by bystander tumor cells (4.5% responding cells vs. 5.1% and 5.7% in the two controls, respectively) (Figures 4A, 4B, and S4B). For NMM tumors, but not for OVCAR5 tumors, it is possible that cytokine-induced cell death results in a slight underestimate of the fraction of cells encountering the combination of IFNγ and TNFα signals. However, for both models, the observed bias toward IFNγ sensing was not predominantly explained by TNFα induced cell death (Figure S4C). Collectively, these data demonstrate in two different mouse models, and using gene sets that either report on the sensing of individual cytokines or on the combination of IFNγ *plus* TNFα, that widespread sensing is restricted to T cell-derived IFNγ.

IFNγ sensing associates with reduced TGFβ sensing

The ability to identify bystander tumor cells that have sensed IFNγ *in vivo* makes it possible to test whether such sensing is associated with additional changes in cell state. To explore this, we used Milo[36] to identify transcriptionally similar cells (so-called neighborhoods) in the mouse NMM melanoma data. 64 out of 128 neighborhoods were enriched for bystander tumor cells derived from T cell-exposed tumors (hereafter referred to as "T cell-exposed neighborhoods") relative to bystander cells from the PBS control condition (Figure 4C) jointly comprising 74.3% of bystander tumor cells from T cell-exposed tumors. As a control, none of these neighborhoods were enriched or depleted for bystander tumor cells derived from T cell treated tumors in which antigen was lacking (Figure 4D, top). As expected, T cell-exposed neighborhoods showed a prominent IFNγ-sensing profile but were also characterized by reduced expression of a second gene set that showed considerable overlap with genes induced by *in vitro* TGFβ stimulation of NMM melanoma cells (Figure 4D). Analysis of selected TGFβ responsive genes from bulk NMM RNA-seq data (Figure S4A bottom panel) showed that a majority of these (47 out of 70) were negatively correlated with T cell pressure (Figure 4E). However, a large fraction of TGFβ induced genes also appeared to show reduced expression upon IFNγ exposure (Figure S4A), making it difficult to unambiguously ascribe this transcriptional response to lowered TGFβ sensing in T cell neighborhoods using solely gene signatures. To disentangle the transcriptional effects of co-occurring cytokines that regulate partly overlapping gene sets, we employed transcriptional deconvolution of cell neighborhoods, aiming to reconstruct their transcriptomes by algorithmically identifying optimal mixing weights of whole-transcriptome bulk RNA-seq profiles (STAR methods), akin to the CIBERSORT approach.[37] A high similarity was observed between control neighborhoods and profiles of TGFβ-stimulated and unstimulated cells. In contrast, T cell-exposed neighborhoods more strongly resembled IFNγ expression profiles (Figure 4F). Notably, omission of TGFβ-exposed reference profiles from this analysis increased reconstruction error and predominantly did so for control neighborhoods (Figure 4G, left). In contrast, exclusion of IFNγ-profiles specifically increased reconstruction error of T cell-exposed

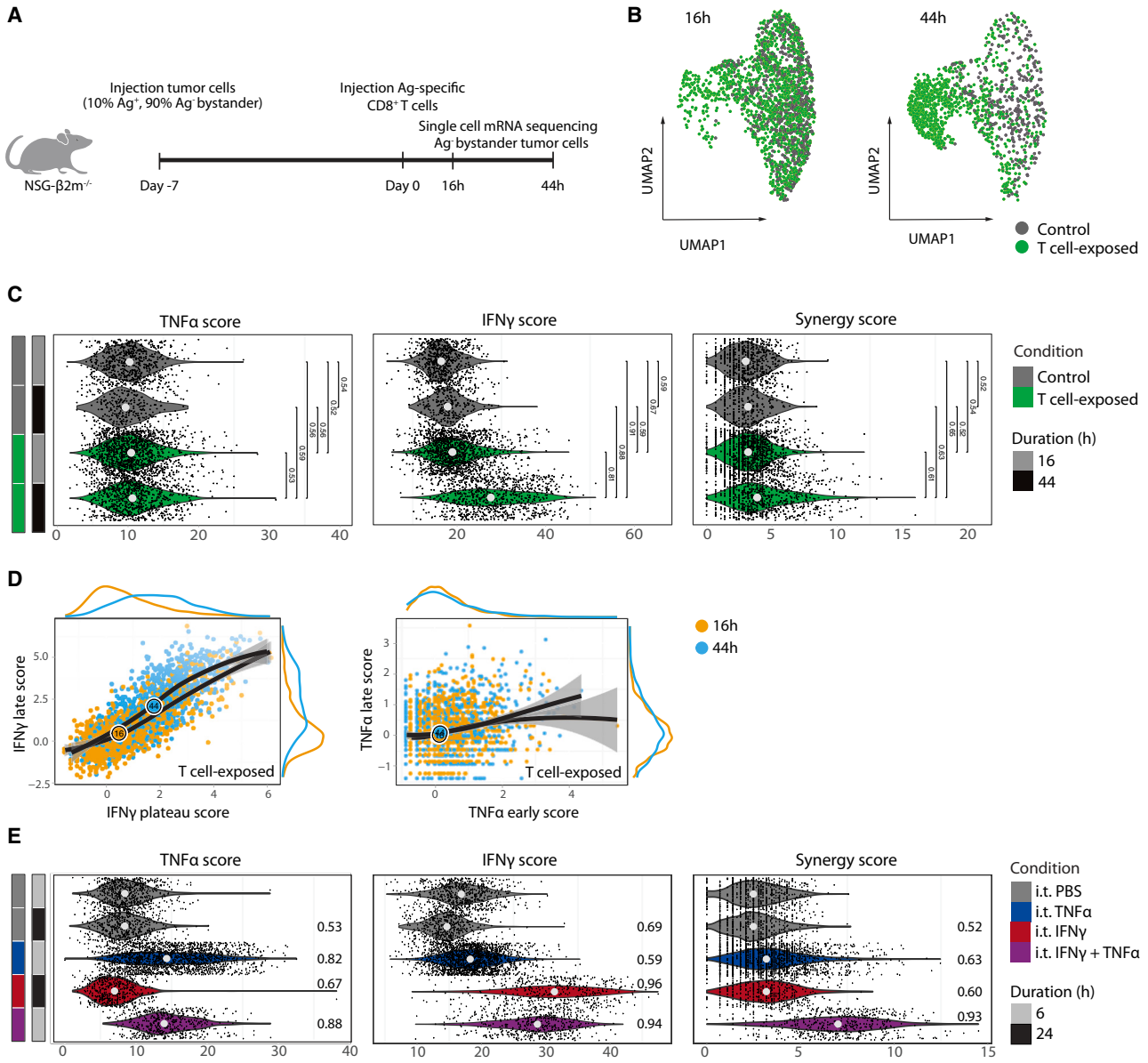

Figure 3. Appreciable IFNγ, but not TNFα sensing by bystander tumor cells early after T cell activation

(A) NSG-β2m$^{-/-}$ mice injected subcutaneously with a mixture of 10% CDK4$_{R>L}$ antigen expressing and 90% bystander OVCAR5 tumor cells were treated with PBS (control) or with CDK4$_{R>L}$-specific CD8$^+$ T cells after tumor establishment. Tumors were harvested 16 or 44 h after treatment, and bystander tumor cells were subjected to scRNA-seq.

(B) UMAP of scRNA-seq from bystander cells of control and T cell-exposed OVCAR5 tumors harvested 16 or 44 h after treatment, based on genes in the "cytokine-responsive" class.

(C) Violin plots of TNFα, IFNγ, and synergy gene set scores of cells derived from OVCAR5 tumors, as described in (A). Dots represent gene set scores of individual cells, violins represent densities of score distributions, white dots represent group medians. Numeric values reflect AUROC values that quantify separability between experimental conditions.

(D) Scatterplots of time-informative gene sets for *in vivo* single cell data described in (A). To remove gene expression effects due to exposure duration independent from T cell exposure, depicted gene set scores were normalized to control (PBS treated) counterparts in a duration-matched fashion (STAR methods).

(E) TNFα, IFNγ, and synergy gene set scores of OVCAR5 tumor cells derived from tumors injected with indicated recombinant cytokines. Cytokine exposure times were chosen based on maximal change in expression of cytokine specific responsive genes after *in vitro* cytokine exposure, as in Figure 1B. Numeric values reflect AUROC values that quantify separability between experimental conditions, as in Figure 1E. See also Figure S3.

CellPress
OPEN ACCESS

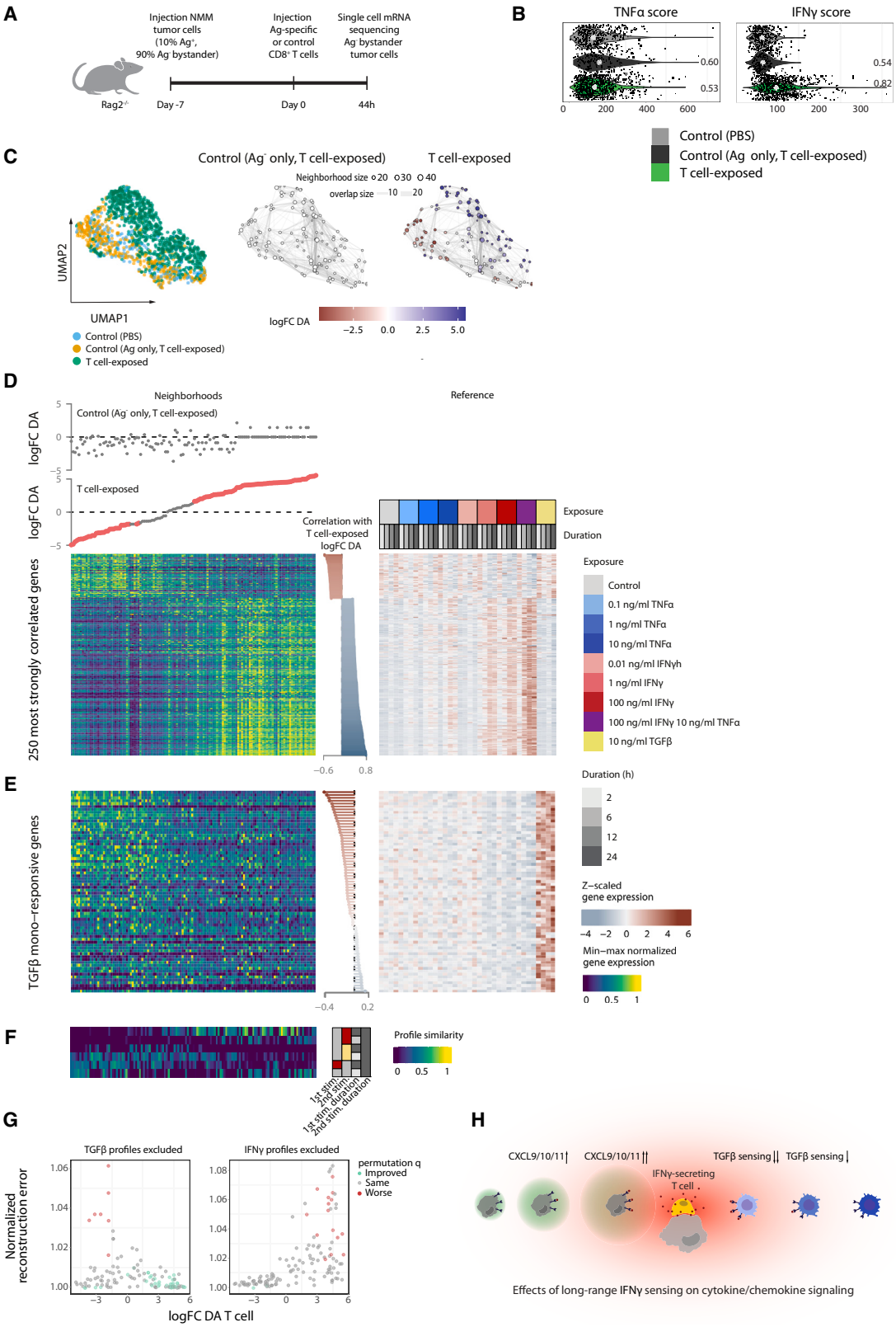

(legend on next page)

neighborhoods (Figure 4G, right). Collectively, these data demonstrate that T cell pressure modulates bystander tumor cells toward transcriptional activity that is consistent with IFNγ--sensing and with reduced TGFβ-sensing.

DISCUSSION

Next to signaling events induced by direct cell-cell contact, tumor cell behavior is modulated through the sensing of soluble mediators, such as chemokines and cytokines, offering possibilities for long range communication. Here, we describe and validate a single cell sequencing-based approach to identify such long-range communication, and also the secondary changes that are associated with it. Key components of this approach are the generation of bespoke gene sets that report on cell exposure to a given cytokine or cytokine combination, and also the employment of multivariate modeling in case signal-specific reporter genes are unavailable. We demonstrate in both humanized and syngeneic tumor models that $CD8^+$ T cells predominantly modulate the behavior of the tumor mass through IFNγ release, while no substantial evidence for widespread TNFα sensing is obtained. This lack of TNFα sensing is observed in spite of ongoing IFNγ sensing by a large fraction of the tumor mass, and hence continuous T cell activity (as a single intratumoral application of IFNγ results in just a transient burst of IFNγ sensing). In addition, we note that bystander tumor cells do retain the capacity to respond to TNFα *in vivo* when this signal is artificially provided. In theory, the methodology that we describe is subject to inferential bias in case the studied signals influence cell survival. In our case, such cell survival effects do not form a significant confounder, but it is important to be aware of this possibility when examining other cell models. The cumulative $CD8^+$ T cell-derived IFNγ and TNFα levels will vary across tumors, depending on e.g., the fraction of tumor cells presenting relevant antigen and T cell density. Importantly though, we consider it likely that, unless local TME signals would differentially influence production of either cytokine, the ratio between T cell produced TNFα and IFNγ will be constant due to their shared dependence on TCR-triggering. Hence, our observation of a differential reach of $CD8^+$ T cell-derived IFNγ and TNFα is expected to generalize to unseen settings.

Prior work has demonstrated that exposure to IFNγ and TNFα can influence tumor control by, for instance, inhibiting growth of antigen loss variants[13,18,29,30] and modifying behavior of tumor stromal cells.[16,38] Here we demonstrate that, whereas T cell-derived IFNγ modulates the behavior of a large fraction of antigen-negative cells in the TME, such global effects are not observed for TNFα. These observations lead us to propose a distinction between cytokines that act as local versus global modifiers of the TME. Importantly, modification of tumor growth through the global TME modifier IFNγ may be expected to already occur in settings in which T cell activity is heterogeneous and restricted to smaller areas of the tumor cell mass. In contrast, the effect of local TME modifiers such as TNFα may be most apparent in case of a stronger and more homogeneous intratumoral T cell response. Notably, should other cell types show a drastically different ratio of IFNγ and TNFα production, it would be of interest to evaluate differential sensing in these settings.

Finally, the ability to detect sensing of individual cytokines and chemokines makes it possible to determine whether such sensing is associated with additional alterations in cell state. In the current work, we demonstrate that cell states induced by T cell activity are not only consistent with abundant IFNγ sensing but also with decreased TGFβ-induced gene expression. Conceivably, intratumoral IFNγ sensing could result in reduced availability of bioactive TGFβ, for instance through induction of a more pro-inflammatory macrophage state[39,40](Figure 4H). In addition, we provide evidence for mutual negative regulation between the two cytokines. These data add to an emerging view on the role of tumor-reactive $CD8^+$ T cells, in which TCR signaling induced cytokine secretion, and in particular IFNγ secretion, results in a global alteration of the tumor micromilieu.

Figure 4. Frequent IFNγ sensing in a syngeneic tumor model and relationship with reduced TGFβ sensing

(A) $Rag2^{-/-}$ mice were injected subcutaneously with a mixture of 10% OVA antigen expressing and 90% Ag^- bystander NMM tumor cells, or with Ag^- NMM tumor cells only, and, following tumor establishment, were treated with either PBS (control) or OT-1 $CD8^+$ T cells, as indicated. Ag^- bystander tumor cells were harvested for scRNA-seq analysis 44 h after treatment.

(B) TNFα and IFNγ gene set scores, determined using the genes shown in a, for the T cell-exposed condition (green) and the two control conditions (T cell-exposed-Ag^- bystander NMM tumor cells only tumors, and PBS treated tumors, shades of gray). Dots represent gene set scores of individual cells, violins represent densities of score distributions, white dots represent group medians.

(C) Left panel: UMAP of NMM melanoma single cell data, as described in (A) and (B). Middle and right panels: a Milo model[36] was fitted to the data to test for enrichment or depletion for any of the experimental conditions in neighborhoods of transcriptionally similar cells. Non-significantly imbalanced neighborhoods (Spatial FDR >0.05), as well as homogeneous neighborhoods, are colored white.

(D) Left panel: heatmap of top 250 genes (rows) most strongly correlated (Spearman correlation) with enrichment for the T cell-exposed condition in cell state neighborhoods (columns) of transcriptionally similar cells. Depicted values are neighborhood averages. Neighborhoods are ordered according to compositional enrichment of cells from the T cell-exposed condition. Top panels show log fold change in differential abundance (logFC DA) for the indicated experimental condition relative to control condition. Right panel: heatmap showing bulk RNA-seq gene expression profiles of NMM cells exposed to indicated cytokines for the same genes as in the heatmap in the left panel, ordered identically.

(E) As in (D), but for TGFβ responsive genes selected on bulk RNA-seq data.

(F) Deconvolution mixing weights of neighborhoods in an independent bulk RNA-seq experiment. Neighborhoods ordered as in (D). Only the 6 out of 28 most highly selected reference profiles are shown, jointly comprising 94% of all assigned similarity.

(G) Left: Increase in reconstruction error when the 17 reference profiles with TGFβ are omitted as compared to when all 28 profiles are included. Permutation testing was employed to test whether increase in reconstruction error could be explained by a lower number of reference profiles (STAR methods). Right: As left, but omitting the 17 reference profiles with IFNγ.

(H) Model visualizing secondary effects of long range IFNγ sensing. In parallel to the mechanism in which long range IFNγ sensing leads to generation of, for instance, CXCL9/10/11 chemokine fields and subsequent increased immune cell infiltration, long range IFNγ sensing may result in secondary changes in the TME by decreasing TGFβ sensing. See also Figure S4.

STAR★METHODS

Detailed methods are provided in the online version of this paper and include the following:

- KEY RESOURCES TABLE
- RESOURCE AVAILABILITY
  - Lead contact
  - Materials availability
  - Data and code availability
- EXPERIMENTAL MODEL AND PARTICIPANT DETAILS
  - Tumor cell culture and viral transductions
  - Mice
- METHOD DETAILS
  - Generation and culture of TCR-modified T cells
  - *In vitro* cytokine stimulation
  - *In vivo* tumor models
  - Intratumoral cytokine injection
  - Flow cytometry
  - Bulk mRNA sequencing
  - Single cell gene expression library generation and sequencing
  - Bulk RNA-seq data preprocessing
  - Selection of cytokine-responsive genes
  - Human ovarian carcinoma single cell sequencing data preprocessing
  - Murine NRAS mutant melanoma single cell sequencing data preprocessing
  - Heatmap visualization of bulk RNA-seq data
  - Gene set scores for single cell data
  - Quantification of separability of experimental conditions using gene set scores
  - Milo neighborhood analysis of single cell data
  - Deconvolution analysis of single cell neighborhood expression
- QUANTIFICATION AND STATISTICAL ANALYSIS

SUPPLEMENTAL INFORMATION

Supplemental information can be found online at https://doi.org/10.1016/j.ccell.2023.12.010.

ACKNOWLEDGMENTS

We thank K. Bresser, A. M. van der Leun, L. Kok and S. Mourragui for input and valuable discussions. We thank staff of the NKI Genomics Core facility for technical support, along with the NKI Research High Performance Computing, Animal Intervention, and Flow Cytometry facilities. This work was supported by a Boehringer Ingelheim Fonds PhD Fellowship (to M.E.H.), ERC AdG SENSIT, grant agreement ID 742259 (to T.N.S.) and institutional funding of the Netherlands Cancer Institute by the Dutch Cancer Society.

AUTHOR CONTRIBUTIONS

M.E.H. conceived the study together with M.S. and T.N.S., performed wet lab experiments and wrote the manuscript with M.S., L.F.A.W. and T.N.S. M.S. performed and interpreted bioinformatic analyses. J.U. and M.T. aided in wet lab experiments. N.S. performed exploratory data analysis. R.K. and M.N., designed and performed sequencing experiments and I.d.R. and R.J.C.K. performed data preprocessing. L.F.A.W. and T.N.S. supervised bioinformatic analyses, and T.N.S. supervised wet-lab experiments. All authors have read and approved the manuscript.

DECLARATION OF INTERESTS

L.F.A.W. received project funding for unrelated work from Bristoll-Myers-Squibb. T.N.S. is advisor for Allogene Therapeutics, Asher Bio, Merus, Neogene Therapeutics, and Scenic Biotech; is a stockholder in Allogene Therapeutics, Asher Bio, Cell Control, Celsius, Merus, and Scenic Biotech; and is venture partner at Third Rock Ventures, all outside of the current work.

Received: December 12, 2022
Revised: October 13, 2023
Accepted: December 12, 2023
Published: January 8, 2024

REFERENCES

1. Giladi, A., Cohen, M., Medaglia, C., Baran, Y., Li, B., Zada, M., Bost, P., Blecher-Gonen, R., Salame, T.M., Mayer, J.U., et al. (2020). Dissecting cellular crosstalk by sequencing physically interacting cells. Nat. Biotechnol. *38*, 629–637.
2. Altan-Bonnet, G., and Mukherjee, R. (2019). Cytokine-mediated communication: a quantitative appraisal of immune complexity. Nat. Rev. Immunol. *19*, 205–217.
3. Raskov, H., Orhan, A., Christensen, J.P., and Gögenur, I. (2021). Cytotoxic CD8(+) T cells in cancer and cancer immunotherapy. Br. J. Cancer *124*, 359–367.
4. Rosenberg, S.A., Yang, J.C., Sherry, R.M., Kammula, U.S., Hughes, M.S., Phan, G.Q., Citrin, D.E., Restifo, N.P., Robbins, P.F., Wunderlich, J.R., et al. (2011). Durable complete responses in heavily pretreated patients with metastatic melanoma using T-cell transfer immunotherapy. Clin. Cancer Res. *17*, 4550–4557.
5. Dudley, M.E., Gross, C.A., Somerville, R.P.T., Hong, Y., Schaub, N.P., Rosati, S.F., White, D.E., Nathan, D., Restifo, N.P., Steinberg, S.M., et al. (2013). Randomized selection design trial evaluating CD8+-enriched versus unselected tumor-infiltrating lymphocytes for adoptive cell therapy for patients with melanoma. J. Clin. Oncol. *31*, 2152–2159.
6. Morotti, M., Albukhari, A., Alsaadi, A., Artibani, M., Brenton, J.D., Curbishley, S.M., Dong, T., Dustin, M.L., Hu, Z., McGranahan, N., et al. (2021). Promises and challenges of adoptive T-cell therapies for solid tumours. Br. J. Cancer *124*, 1759–1776.
7. Mojic, M., Takeda, K., and Hayakawa, Y. (2017). The Dark Side of IFN-gamma: Its Role in Promoting Cancer Immunoevasion. Int. J. Mol. Sci. *19*, 89.
8. Castro, F., Cardoso, A.P., Gonçalves, R.M., Serre, K., and Oliveira, M.J. (2018). Interferon-Gamma at the Crossroads of Tumor Immune Surveillance or Evasion. Front. Immunol. *9*, 847.
9. Mosser, D.M., and Edwards, J.P. (2008). Exploring the full spectrum of macrophage activation. Nat. Rev. Immunol. *8*, 958–969.
10. Jorgovanovic, D., Song, M., Wang, L., and Zhang, Y. (2020). Roles of IFN-gamma in tumor progression and regression: a review. Biomark. Res. *8*, 49.
11. Parameswaran, N., and Patial, S. (2010). Tumor necrosis factor-alpha signaling in macrophages. Crit. Rev. Eukaryot. Gene Expr. *20*, 87–103.
12. Trevejo, J.M., Marino, M.W., Philpott, N., Josien, R., Richards, E.C., Elkon, K.B., and Falck-Pedersen, E. (2001). TNF-alpha -dependent maturation of local dendritic cells is critical for activating the adaptive immune response to virus infection. Proc. Natl. Acad. Sci. USA *98*, 12162–12167.
13. Braumüller, H., Wieder, T., Brenner, E., Aßmann, S., Hahn, M., Alkhaled, M., Schilbach, K., Essmann, F., Kneilling, M., Griessinger, C., et al. (2013). T-helper-1-cell cytokines drive cancer into senescence. Nature *494*, 361–365.
14. Montfort, A., Colacios, C., Levade, T., Andrieu-Abadie, N., Meyer, N., and Ségui, B. (2019). The TNF Paradox in Cancer Progression and Immunotherapy. Front. Immunol. *10*, 1818.

15. Wang, W., Green, M., Choi, J.E., Gijón, M., Kennedy, P.D., Johnson, J.K., Liao, P., Lang, X., Kryczek, I., Sell, A., et al. (2019). CD8(+) T cells regulate tumour ferroptosis during cancer immunotherapy. Nature *569*, 270–274.

16. Kammertoens, T., Friese, C., Arina, A., Idel, C., Briesemeister, D., Rothe, M., Ivanov, A., Szymborska, A., Patone, G., Kunz, S., et al. (2017). Tumour ischaemia by interferon-gamma resembles physiological blood vessel regression. Nature *545*, 98–102.

17. Briesemeister, D., Sommermeyer, D., Loddenkemper, C., Loew, R., Uckert, W., Blankenstein, T., and Kammertoens, T. (2011). Tumor rejection by local interferon gamma induction in established tumors is associated with blood vessel destruction and necrosis. Int. J. Cancer *128*, 371–378.

18. Zhang, B., Karrison, T., Rowley, D.A., and Schreiber, H. (2008). IFN-gamma- and TNF-dependent bystander eradication of antigen-loss variants in established mouse cancers. J. Clin. Invest. *118*, 1398–1404.

19. Spiotto, M.T., Rowley, D.A., and Schreiber, H. (2004). Bystander elimination of antigen loss variants in established tumors. Nat. Med. *10*, 294–298.

20. Spiotto, M.T., and Schreiber, H. (2005). Rapid destruction of the tumor microenvironment by CTLs recognizing cancer-specific antigens cross-presented by stromal cells. Cancer Immun. *5*, 8.

21. Huse, M., Lillemeier, B.F., Kuhns, M.S., Chen, D.S., and Davis, M.M. (2006). T cells use two directionally distinct pathways for cytokine secretion. Nat. Immunol. *7*, 247–255.

22. Kupfer, A., Mosmann, T.R., and Kupfer, H. (1991). Polarized expression of cytokines in cell conjugates of helper T cells and splenic B cells. Proc. Natl. Acad. Sci. USA *88*, 775–779.

23. Sanderson, N.S.R., Puntel, M., Kroeger, K.M., Bondale, N.S., Swerdlow, M., Iranmanesh, N., Yagita, H., Ibrahim, A., Castro, M.G., and Lowenstein, P.R. (2012). Cytotoxic immunological synapses do not restrict the action of interferon-gamma to antigenic target cells. Proc. Natl. Acad. Sci. USA *109*, 7835–7840.

24. Hoekstra, M.E., Vijver, S.V., and Schumacher, T.N. (2021). Modulation of the tumor micro-environment by CD8(+) T cell-derived cytokines. Curr. Opin. Immunol. *69*, 65–71.

25. Perona-Wright, G., Mohrs, K., and Mohrs, M. (2010). Sustained signaling by canonical helper T cell cytokines throughout the reactive lymph node. Nat. Immunol. *11*, 520–526.

26. Ariotti, S., Hogenbirk, M.A., Dijkgraaf, F.E., Visser, L.L., Hoekstra, M.E., Song, J.Y., Jacobs, H., Haanen, J.B., and Schumacher, T.N. (2014). T cell memory. Skin-resident memory CD8(+) T cells trigger a state of tissue-wide pathogen alert. Science *346*, 101–105.

27. Schenkel, J.M., Fraser, K.A., Beura, L.K., Pauken, K.E., Vezys, V., and Masopust, D. (2014). T cell memory. Resident memory CD8 T cells trigger protective innate and adaptive immune responses. Science *346*, 98–101.

28. Müller, A.J., Filipe-Santos, O., Eberl, G., Aebischer, T., Späth, G.F., and Bousso, P. (2012). CD4+ T cells rely on a cytokine gradient to control intracellular pathogens beyond sites of antigen presentation. Immunity *37*, 147–157.

29. Thibaut, R., Bost, P., Milo, I., Cazaux, M., Lemaître, F., Garcia, Z., Amit, I., Breart, B., Cornuot, C., Schwikowski, B., and Bousso, P. (2020). Bystander IFN-gamma activity promotes widespread and sustained cytokine signaling altering the tumor microenvironment. Nat. Can. (Ott.) *1*, 302–314.

30. Hoekstra, M.E., Bornes, L., Dijkgraaf, F.E., Philips, D., Pardieck, I.N., Toebes, M., Thommen, D.S., van Rheenen, J., and Schumacher, T.N.M. (2020). Long-distance modulation of bystander tumor cells by CD8(+) T cell-secreted IFNgamma. Nat. Can. (Ott.) *1*, 291–301.

31. Beck, R.J., Slagter, M., and Beltman, J.B. (2019). Contact-Dependent Killing by Cytotoxic T Lymphocytes Is Insufficient for EL4 Tumor Regression In Vivo. Cancer Res. *79*, 3406–3416.

32. Liberzon, A., Birger, C., Thorvaldsdóttir, H., Ghandi, M., Mesirov, J.P., and Tamayo, P. (2015). The Molecular Signatures Database (MSigDB) hallmark gene set collection. Cell Syst. *1*, 417–425.

33. Büttner, M., Miao, Z., Wolf, F.A., Teichmann, S.A., and Theis, F.J. (2019). A test metric for assessing single-cell RNA-seq batch correction. Nat. Methods *16*, 43–49.

34. Fukunaga, R., Sokawa, Y., and Nagata, S. (1984). Constitutive production of human interferons by mouse cells with bovine papillomavirus as a vector. Proc. Natl. Acad. Sci. USA *81*, 5086–5090.

35. Savan, R., Ravichandran, S., Collins, J.R., Sakai, M., and Young, H.A. (2009). Structural conservation of interferon gamma among vertebrates. Cytokine Growth Factor Rev. *20*, 115–124.

36. Dann, E., Henderson, N.C., Teichmann, S.A., Morgan, M.D., and Marioni, J.C. (2022). Differential abundance testing on single-cell data using k-nearest neighbor graphs. Nat. Biotechnol. *40*, 245–253.

37. Newman, A.M., Liu, C.L., Green, M.R., Gentles, A.J., Feng, W., Xu, Y., Hoang, C.D., Diehn, M., and Alizadeh, A.A. (2015). Robust enumeration of cell subsets from tissue expression profiles. Nat. Methods *12*, 453–457.

38. Garnier, L., Pick, R., Montorfani, J., Sun, M., Brighouse, D., Liaudet, N., Kammertoens, T., Blankenstein, T., Page, N., Bernier-Latamani, J., et al. (2022). IFN-gamma-dependent tumor-antigen cross-presentation by lymphatic endothelial cells promotes their killing by T cells and inhibits metastasis. Sci. Adv. *8*, eabl5162.

39. Boutilier, A.J., and Elsawa, S.F. (2021). Macrophage Polarization States in the Tumor Microenvironment. Int. J. Mol. Sci. *22*, 6995.

40. Wen, F.Q., Kohyama, T., Liu, X., Zhu, Y.K., Wang, H., Kim, H.J., Kobayashi, T., Abe, S., Spurzem, J.R., and Rennard, S.I. (2002). Interleukin-4- and interleukin-13-enhanced transforming growth factor-beta2 production in cultured human bronchial epithelial cells is attenuated by interferon-gamma. Am. J. Respir. Cell Mol. Biol. *26*, 484–490.

41. Burd, C.E., Liu, W., Huynh, M.V., Waqas, M.A., Gillahan, J.E., Clark, K.S., Fu, K., Martin, B.L., Jeck, W.R., Souroullas, G.P., et al. (2014). Mutation-specific RAS oncogenicity explains NRAS codon 61 selection in melanoma. Cancer Discov. *4*, 1418–1429.

42. Vredevoogd, D.W., Kuilman, T., Ligtenberg, M.A., Boshuizen, J., Stecker, K.E., de Bruijn, B., Krijgsman, O., Huang, X., Kenski, J.C.N., Lacroix, R., et al. (2019). Augmenting Immunotherapy Impact by Lowering Tumor TNF Cytotoxicity Threshold. Cell *178*, 585–599.e15.

43. van Rooij, N., van Buuren, M.M., Philips, D., Velds, A., Toebes, M., Heemskerk, B., van Dijk, L.J.A., Behjati, S., Hilkmann, H., El Atmioui, D., et al. (2013). Tumor exome analysis reveals neoantigen-specific T-cell reactivity in an ipilimumab-responsive melanoma. J. Clin. Oncol. *31*, e439–e442.

44. Hafemeister, C., and Satija, R. (2019). Normalization and variance stabilization of single-cell RNA-seq data using regularized negative binomial regression. Genome Biol. *20*, 296.

45. Kim, D., Paggi, J.M., Park, C., Bennett, C., and Salzberg, S.L. (2019). Graph-based genome alignment and genotyping with HISAT2 and HISAT-genotype. Nat. Biotechnol. *37*, 907–915.

46. Law, C.W., Chen, Y., Shi, W., and Smyth, G.K. (2014). voom: Precision weights unlock linear model analysis tools for RNA-seq read counts. Genome Biol. *15*, R29.

47. Gillespie, M., Jassal, B., Stephan, R., Milacic, M., Rothfels, K., Senff-Ribeiro, A., Griss, J., Sevilla, C., Matthews, L., Gong, C., et al. (2022). The reactome pathway knowledgebase 2022. Nucleic Acids Res. *50*, D687–D692.

48. Friedman, J., Hastie, T., and Tibshirani, R. (2010). Regularization Paths for Generalized Linear Models via Coordinate Descent. J. Stat. Software *33*, 1–22.

49. Landau, W. (2021). The targets R package: a dynamic Make-like function-oriented pipeline toolkit for reproducibility and high-performance computing. J. Open Source Softw. *6*, 2959.

50. Wickham, H., Hester, J., Chang, W., and Bryan, J. (2022). Devtools: Tools to Make Developing R Packages Easier. R package version 2.4.5. https://CRAN.R-project.org/package=devtools.

51. Gu, Z., Eils, R., and Schlesner, M. (2016). Complex heatmaps reveal patterns and correlations in multidimensional genomic data. Bioinformatics *32*, 2847–2849.

52. Ooms, J. (2021). Credentials: Tools for Managing SSH and Git Credentials. R Package version 1.3.2. https://CRAN.R-project.org/package=credentials.

53. Morgan, M., and Dann, E. (2021). miloR: Differential Neighbourhood Abundance Testing on a Graph. R Package Version 1.0.0. https://marionilab.github.io/miloR.

54. Fox, J., and Weisberg, S. (2019). An R Companion to Applied Regression, Third edition (Sage). https://socialsciences.mcmaster.ca/jfox/Books/Companion/.

55. Kuhn, M., and Vaughan, D. (2022). Parsnip: A Common API to Modeling and Analysis Functions. R package version 1.0.3. https://CRAN.R-project.org/package=parsnip.

56. Kuhn, M., and Wickham, H. (2020). Tidymodels: A Collection of Packages for Modeling and Machine Learning Using Tidyverse Principles. https://www.tidymodels.org.

57. Kuhn, M., Vaughan, D., and Hvitfeldt, E. (2022). Yardstick: Tidy Characterizations of Model Performance. R Package Version 1.1.0. https://CRAN.R-project.org/package=yardstick.

58. Wright, M.N., and Ziegler, A. (2017). ranger: A Fast Implementation of Random Forests for High Dimensional Data in C++ and R. J. Stat. Software *77*, 1–17.

59. Schliep, K., and Hechenbichler, K. (2016). Kknn: Weighted K-Nearest Neighbors. R package version 1.3.1. https://CRAN.R-project.org/package=kknn.

60. Ooms, J. (2023). Curl: A Modern and Flexible Web Client for R. R Package Version 5.0.0. https://CRAN.R-project.org/package=curl.

61. Kassambara, A. (2023). Ggpubr: 'ggplot2' Based Publication Ready Plots. R package version 0.6.0. https://CRAN.R-project.org/package=ggpubr.

62. Kauffmann, A., Rayner, T.F., Parkinson, H., Kapushesky, M., Lukk, M., Brazma, A., and Huber, W. (2009). Importing ArrayExpress datasets into R/Bioconductor. Bioinformatics *25*, 2092–2094.

63. Konopka, T. (2023). Umap: Uniform Manifold Approximation and Projection. R Package Version 0.2.10.0. https://CRAN.R-project.org/package=umap.

64. Bengtsson, H. (2023). Progressr: An Inclusive, Unifying API for Progress Updates. R Package Version 0.13.0. https://CRAN.R-project.org/package=progressr.

65. Frick, H., Chow, F., Kuhn, M., Mahoney, M., Silge, J., and Wickham, H. (2022). Rsample: General Resampling Infrastructure. R Package version 1.1.1. https://CRAN.R-project.org/package=rsample.

66. Harrell, F., Jr. (2023). Hmisc: Harrell Miscellaneous. R Package Version 4.8-0. https://CRAN.R-project.org/package=Hmisc.

67. Bolstad, B.. preprocessCore: A Collection of Pre-processing Functions. R Package Version 1.57.0. https://github.com/bmbolstad/preprocessCore.

68. Mastropietro, D. (2020). Envnames: Keep Track of User-Defined Environment Names. R package version 0.4.1. https://CRAN.R-project.org/package=envnames.

69. Borchers, H. (2022). Pracma: Practical Numerical Math Functions. R package version 2.4.2. https://CRAN.R-project.org/package=pracma.

70. Love, M.I., Huber, W., and Anders, S. (2014). Moderated estimation of fold change and dispersion for RNA-seq data with DESeq2. Genome Biol. *15*, 550.

71. Ram, K., and Wickham, H. (2018). Wesanderson: A Wes Anderson Palette Generator. R package version 0.3.6. https://CRAN.R-project.org/package=wesanderson.

72. Durinck, S., Spellman, P.T., Birney, E., and Huber, W. (2009). Mapping identifiers for the integration of genomic datasets with the R/Bioconductor package biomaRt. Nat. Protoc. *4*, 1184–1191.

73. Vaughan, D., and Dancho, M. (2022). Furrr: Apply Mapping Functions in Parallel Using Futures. R package version 0.3.1. https://CRAN.R-project.org/package=furrr.

74. Korotkevich, G., Sukhov, V., Budin, N., Shpak, B., Artyomov, M.N., and Sergushichev, A. (2019). Fast gene set enrichment analysis. Preprint at bioRxiv *10*.

75. Abe, K. (2016). Naturalsort: Natural Ordering. R package version 0.1.3. https://CRAN.R-project.org/package=naturalsort.

76. Wickham, H., Averick, M., Bryan, J., Chang, W., McGowan, L., François, R., Grolemund, G., Hayes, A., Henry, L., Hester, J., et al. (2019). Welcome to the tidyverse. J. Open Source Softw. *4*, 1686.

77. Xie, Y. (2023). Knitr: A General-Purpose Package for Dynamic Report Generation in R. R Package version 1.42. https://yihui.org/knitr/.

78. Sharpsteen, C., and Bracken, C. (2023). tikzDevice: R Graphics Output in LaTeX Format. R package version 0.12.4. https://CRAN.R-project.org/package=tikzDevice.

79. Lun, A.T.L., McCarthy, D.J., and Marioni, J.C. (2016). A step-by-step workflow for low-level analysis of single-cell RNA-seq data with Bioconductor. F1000Res. *5*, 2122.

80. Amezquita, R.A., Lun, A.T.L., Becht, E., Carey, V.J., Carpp, L.N., Geistlinger, L., Marini, F., Rue-Albrecht, K., Risso, D., Soneson, C., et al. (2020). Orchestrating single-cell analysis with Bioconductor. Nat. Methods *17*, 137–145. https://www.nature.com/articles/s41592-019-0654.

81. Ritchie, M.E., Phipson, B., Wu, D., Hu, Y., Law, C.W., Shi, W., and Smyth, G.K. (2015). limma powers differential expression analyses for RNA-sequencing and microarray studies. Nucleic Acids Res. *43*, e47.

82. Robinson, M.D., McCarthy, D.J., and Smyth, G.K. (2010). edgeR: a Bioconductor package for differential expression analysis of digital gene expression data. Bioinformatics *26*, 139–140.

83. Sing, T., Sander, O., Beerenwinkel, N., and Lengauer, T. (2005). ROCR: visualizing classifier performance in R. Bioinformatics *21*, 3940–3941. http://rocr.bioinf.mpi-sb.mpg.de.

84. Hao, Y., Hao, S., Andersen-Nissen, E., Mauck, W.M., 3rd, Zheng, S., Butler, A., Lee, M.J., Wilk, A.J., Darby, C., Zager, M., et al. (2021). Integrated analysis of multimodal single-cell data. Cell *184*, 3573–3587.e29.

85. Schloerke, B., Cook, D., Larmarange, J., Briatte, F., Marbach, M., Thoen, E., Elberg, A., and Crowley, J. (2021). GGally: Extension to 'ggplot2'. R Package Version 2.1.2. https://CRAN.R-project.org/package=GGally.

86. Rinker, T.W., and Kurkiewicz, D. (2018). Pacman: Package Management for R. Version 0.5.0. http://github.com/trinker/pacman.

87. Gu, Z., Gu, L., Eils, R., Schlesner, M., and Brors, B. (2014). circlize implements and enhances circular visualization in R. Bioinformatics *30*, 2811–2812.

88. Gaujoux, R., and Seoighe, C. (2010). A flexible R package for nonnegative matrix factorization. BMC Bioinf. *11*, 367.

89. Meyer, D., Dimitriadou, E., Hornik, K., Weingessel, A., and Leisch, F. (2023). e1071: Misc Functions of the Department of Statistics, Probability Theory Group (Formerly: E1071), TU Wien. R package version 1.7-13. https://CRAN.R-project.org/package=e107.

90. Ewels, P.A., Peltzer, A., Fillinger, S., Patel, H., Alneberg, J., Wilm, A., Garcia, M.U., Di Tommaso, P., and Nahnsen, S. (2020). Alexander Peltzer, Sven Fillinger, Harshil Patel, Johannes Alneberg, Andreas Wilm, Maxime Ulysse Garcia, Paolo Di Tommaso, and Sven Nahnsen. "The Nf-Core Framework for Community-Curated Bioinformatics Pipelines.". Nat. Biotechnol. *38*, 276–278.

91. Bray, N.L., Pimentel, H., Melsted, P., Melsted, P., and Pachter, L. (2016). Near-Optimal Probabilistic RNA-Seq Quantification. Nat. Biotechnol. *34*, 525–527.

92. R Core Team (2021). R: A Language and Environment for Statistical Computing (R Foundation for Statistical Computing). https://www.R-project.org.

STAR★METHODS

KEY RESOURCES TABLE

REAGENT or RESOURCE	SOURCE	IDENTIFIER
Antibodies		
Mouse anti-human CD3 antibody	BD biosciences	clone OKT3, RRID: AB_2869821
Hamster anti-mouse TCRβ constant domain	BD biosciences	clone H57-597 RRID: AB_394679
Mouse anti-human IFNγ	BD biosciences	clone 4S.B3 RRID: AB_398569
Mouse anti-human TNFα	eBioscience	clone MAb11 RRID: AB_468489
TotalSeq Hashtag anti-human antibodies	Biolegend	CAT#: 394631; 394633; 394635; 394637; 394639; 394641; 394643; 394645; 394647; 394649
TotalSeq Hashtag anti-mouse antibodies	Biolegend	CAT#: 155831; 155833; 155835; 155837; 155839; 155841; 155843; 155845; 155847; 155849
Bacterial and virus strains		
pMP71-CDK4R > L TCR (retroviral)	van Rooij et al.[43]	N/A
CDK4R > L-GFP-pMX (retroviral)	Hoekstra et al.[30]	N/A
CFP-pMX (retroviral)	Hoekstra et al.[30]	N/A
IGS-PCDH (lentiviral)	Hoekstra et al.[30]	N/A
OVA-mPlumb-pLenti (lentiviral)	Vredevoogd et al.[42]	N/A
Chemicals, peptides, and recombinant proteins		
Recombinant human IFNγ	Invitrogen	CAT#: RP-8607
Recombinant human TNFα	Peprotech	CAT#: 300-01A
Recombinant murine IFNγ	Thermo Fisher	CAT#: BMS326
Recombinant murine TNFα	Peprotech	CAT#: 315-01A
Recombinant murine TGFβ	ebioscience	CAT#: 14-8342-80
Recombinant human IL-2	Immunotools	CAT#: 11340027
Recombinant human IL-7	Immunotools	CAT#: 11340077
Recombinant human IL-15	Immunotools	CAT#: 11340155
Recombinant human IL-2 (Proleukin)	Novartis	N/A
Matrigel (Basement Membrane Matrix)	Corning	CAT#: 354234
Critical commercial assays		
xGen™ RNA Lib Prep 96rxn	IDT	CAT#: 10009814
RNeasy Mini Kit	Qiagen)	CAT#: 74106
On-column DNase digestion kit	Qiagen	CAT#: 79254
Agilent DNA 7500 kit	Agilent Technologies	CAT#: G2938-90024
Agilent RNA 6000 Nano kit	Agilent Technologies	CAT#: G2938-90034
HiSeq SR Cluster Kit v4 cBot	Illumina	CAT#: GD-401-4001
HiSeq SBS Kit V4 50 cycle kit	Illumina	CAT#: FC-401-4002
NovaSeq 6000 SP Reagent Kit v1.5	Illumina	CAT#: 20028401
KAPA Library Quantification Kit	KAPA Biosystems	CAT#: KR0405
HiSeq PE Cluster Kit V4	Illumina	CAT#: PE-401-4001
HiSeq SBS Kit V4 50 cycle kit	Illumina	CAT#: FC-401-4002
NextSeq 500/550 High Output Kit v2.5	Illumina	CAT#: 20024906

(*Continued on next page*)

Continued

REAGENT or RESOURCE	SOURCE	IDENTIFIER
NextSeq 500/550 Mid Output Kit v2.5	Illumina	CAT#: 20024904
NovaSeq 6000 S2 Reagent Kit v1.5	Illumina	CAT#: 20028316
Deposited data		
Raw sequencing data and metadata	This paper	GEO: GSE220738
Preprocessed version of sequencing data	This paper, hosted on Mendeley	https://doi.org/10.17632/2wwjdppm7f.2
Experimental models: Cell lines		
Human ovarian carcinoma 5 (OVCAR5) cells	(F. Scheeren, The Netherlands Cancer Institute, The Netherlands)	N/A
murine $NRAS^{Q61R}$ mutant melanoma (NMM) cells	Norman Sharpless, University of North Carolina, USA[41]	N/A
Experimental models: Organisms/strains		
Mouse: NOD-scid $Il2ry^{null}B2m^{null}$ (NSG-$\beta2m^{-/-}$)	Jackson Laboratories	Strain #:010636
Mouse: C57BL/6; RAG2 KO mouse	Jackson Laboratories	Strain #:008449
Mouse: C57BL/6; UBC-GFP mouse	Crossed in house	N/A
Mouse: C57BL/6; OT-I mouse	Crossed in house	N/A
Oligonucleotides		
N/A	N/A	N/A
Recombinant DNA		
See under "bacteria and viral strains" subheading		
Software and algorithms		
GraphPad Prism version 9		
R package devtools 2.4.5	Wickham et al. [50]	https://CRAN.R-project.org/package=devtools
R package ComplexHeatmap 2.9.3	Gu et al. [51]	N/A
R package credentials 1.3.2	Ooms et al. [52]	https://CRAN.R-project.org/package=credentials
R package miloR 1.0.0	Morgan et al. [36,53]	https://marionilab.github.io/miloR
R package car 3.1.1	Fox et al. [54]	https://socialsciences.mcmaster.ca/jfox/Books/Companion/
R package parsnip 1.0.3	Kuhn et al. [55]	https://CRAN.R-project.org/package=parsnip
R package tidymodels 1.0.0	Kuhn et al. [56]	https://www.tidymodels.org
R package yardstick 0.0.9	Kuhn et al. [57]	https://CRAN.R-project.org/package=yardstick
R package ranger 0.14.1	Wright et al. [58]	N/A
R package kknn 1.3.1	Schliep et al. [59]	https://CRAN.R-project.org/package=kknn
R package curl 5.0.0	Ooms et al. [60]	https://CRAN.R-project.org/package=curl
R package ggpubr 0.6.0	Kassambara et al. [61]	https://CRAN.R-project.org/package=ggpubr
R package ArrayExpress 1.52.0	Kauffmann et al. [62]	N/A
R package umap 0.2.10.0	Konopka et al. [63]	https://CRAN.R-project.org/package=umap
R package progressr 0.13.0	Bengtsson et al. [64]	https://CRAN.R-project.org/package=progressr
R package rsample 1.1.1	Frick et al. [65]	https://CRAN.R-project.org/package=rsample
R package Hmisc 4.8.0	Harrell Jr et al. [66]	https://CRAN.R-project.org/package=Hmisc
R package preprocessCore 1.57.0	Bolstad et al. (?)[67]	https://github.com/bmbolstad/preprocessCore
R package envnames 0.4.1	Mastropietro et al. [68]	https://CRAN.R-project.org/package=envnames
R package pracma 2.4.2	Borchers et al. [69]	https://CRAN.R-project.org/package=pracma
R package DESeq2 1.32.0	Love et al. [70]	N/A
R package wesanderson 0.3.6	Ram et al. [71]	https://CRAN.R-project.org/package=wesanderson
R package biomaRt 2.48.3	Durinck et al. [72]	N/A
R package furrr 0.3.1	Vaughan et al. [73]	https://CRAN.R-project.org/package=furrr
R package fgsea 1.18.0	Korotkevich et al. [74]	http://biorxiv.org/content/early/2016/06/20/060012

(*Continued on next page*)

Continued

REAGENT or RESOURCE	SOURCE	IDENTIFIER
R package naturalsort 0.1.3	Abe et al. [75]	https://CRAN.R-project.org/package=naturalsort
R package tidyverse 1.3.2	Wickham et al. [76]	http://www.tidyverse.org
R package knitr 1.42	Yihui Xie [77]	https://yihui.org/knitr/
R package tikzDevice 0.12.4	Sharpsteen et al. [78]	https://CRAN.R-project.org/package=tikzDevice
R package scran 1.20.1	Lun et al. [79]	N/A
R package SingleCellExperiment 1.14.1	Amezquita et al. [80]	https://www.nature.com/articles/s41592-019-0654-x
R package limma 3.50.1	Ritchie et al. [81]	N/A
R package edgeR 3.36.0	Robinson et al. [82]	N/A
R package ROCR 1.0.11	Sing et al. [83]	http://rocr.bioinf.mpi-sb.mpg.de
R package Seurat 4.3.0	Hao et al. [84]	https://doi.org/10.1016/j.cell.2021.04.048
R package GGally 2.1.2	Schloerke et al. [85]	https://CRAN.R-project.org/package=GGally
R package pacman 0.5.1	Rinker et al. [86]	http://github.com/trinker/pacman
R package circlize 0.4.15	Gu et al. [87]	N/A
R package NMF 0.25	Renaud et al. [88]	https://bmcbioinformatics.biomedcentral.com/articles/10.1186/1471-2105-11-367
R package e1071 1.7.13	Meyer et al. [89]	https://CRAN.R-project.org/package=e1071
Nextflow core kallisto pipeline version 0.9	Ewels et al. [90]	https://doi.org/10.5281/zenodo.1400710
Kallisto version 0.46.2	Bray et al. [91]	https://doi.org/10.1038/nbt.3519
R programming language, version 4.1	R Core Team [92]	https://www.R-project.org/
R package targets 0.14.2	Landau et al. [49]	https://doi.org/10.21105/joss.02959
R package glmnet 4.1.6	Friedman et al., [48]	https://www.jstatsoft.org/v33/i01/
R package SCTransform 0.3.5	Hafemeister et al., [44]	https://doi.org/10.1186/s13059-019-1874-1
itreecount	N/A	https://github.com/NKI-GCF/itreecount
All code to reproduce the analyses and figures	This paper	https://doi.org/10.5281/zenodo.10142533

RESOURCE AVAILABILITY

Lead contact

Further information and requests for resources and reagents should be directed to and will be fulfilled by the lead contact, T.N. Schumacher (t.schumacher@nki.nl).

Materials availability

This study did not generate new unique reagents.

Data and code availability

- Raw bulk and single-cell RNA-seq data have been deposited at GEO and are publicly available as of the date of publication. Accession numbers are listed in the key resources table. Preprocessed bulk and single-cell RNA-seq have been deposited at Mendeley Data and are publicly available as of the date of publication. The DOI is listed in the key resources table.
- All original code has been deposited at Zenodo and is publicly available as of the date of publication. The DOI is listed in the key resources table.
- Any additional information required to reanalyze the data reported in this paper is available from the lead contact upon request

EXPERIMENTAL MODEL AND PARTICIPANT DETAILS

Tumor cell culture and viral transductions

Human OVCAR5 OVCAR5 cells (F. Scheeren, The Netherlands Cancer Institute, The Netherlands) and murine $NRAS^{Q61R}$ mutant melanoma cells (NMM) (Norman Sharpless, University of North Carolina, USA,[41]) were cultured at 37°C/5% CO_2 in IMDM (Gibco) supplemented with 10% FCS (Sigma), 100 U/ml penicillin (Roche), 100 μg/mL streptomycin (Roche), and GlutaMax (Gibco, 1x). Identity of OVCAR5 cells was validated by short tandem repeat analysis, STR data were not available for the NMM cell line. The following vectors were utilized: the $CDK4_{R>L}$-GFP-pMX, CFP-pMX, and IGS-PCDH vectors as described in,[30] the OVA-mPlumb-pLenti vector

as described in,[42] and the $CDK4_{R>L}$ specific TCR (clone 17, NKI12)- pMP71 vector, as described in.[43] For retroviral transduction of human cells and mouse cells, FLYRD18 packaging cells (ECACC no. 95091902), and Phoenix-ECO packaging cells (ATCC, CRL-3214), were plated into 6 well plate dishes at 0.5×10^6 cells per well, respectively. After 24 h, cells were transfected with 3 μg of one of the indicated retroviral vectors using X-tremeGENE (Roche), according to the manufacturer's protocol. After 48 h, virus supernatant was harvested, filtered through a 0.45-μm filter and added to tumor cells in the presence of 8 μg/mL polybrene (Sigma) in a 1:1 dilution in medium. For lentiviral transductions, HEK293T cells (ATCC, CRL-3216) were plated at $3x10^6$ cells per 10 cm dish. After 24 h, cells were transfected with 8 μg of one of the above indicated lentiviral plasmids, plus the lentiviral packaging and envelope plasmids psPAX (Addgene #12260) and pMD2.G (Addgene #12259) (3 μg each) using X-tremeGENE (Roche), according to the manufacturer's protocol. 2–3 days after transfection, supernatant of transfected cells was harvested, filtered through 0.45-μm filters, and added to OVCAR5 or NMM cells in a 1:1 dilution in medium. Antigen-positive GFP^+ OVCAR5 cells were generated by retroviral transduction with the pMX-$CDK4_{R>L}$-GFP vector. Antigen-positive $mPlumb^+$ NMM cells were generated by lentiviral transduction with the pLenti-OVA-mPlumb vector. Antigen-negative CFP^+ bystander OVCAR5 and NMM cells were generated by retroviral transduction with the pMX-CFP vector. After transduction, indicated cell populations were sorted on a FACSaria Fusion (BD biosciences) to >90% purity. Ag^-CFP^+IGS reporter cells were generated as described.[30]

Mice

NOD-scid $Il2ry^{null}B2m^{null}$ (NSG-$\beta2m^{-/-}$), C57BL/6; RAG2 KO, C57BL/6; UBC-GFP, and C57BL/6; OT-I mice were obtained from Jackson Laboratories. UBC-GFP and OT-I mice were crossed to obtain GFP-OT-I donor mice for adoptive cell transfer experiments. All animal experiments were approved by the Animal Welfare Committee of The Netherlands Cancer Institute (NKI), in accordance with national guidelines. All animals were maintained in the animal department of NKI, housed in individually ventilated cage systems under specific pathogen-free conditions and received food and water *ad libitum*. Mice were used at 8 to 26 weeks of age. Animals of the same sex were randomly assigned to experimental groups, both male and female mice were used in this study.

METHOD DETAILS

Generation and culture of TCR-modified T cells

Retroviral transduction and culture of human T cells was performed as described previously.[30] To obtain murine GFP^+ OT-1 $CD8^+$ T cells, spleens from C57BL/6; UBC-GFP; OT-I mice were passed through 70 μm strainers (Falcon) to obtain single cell suspensions. Splenocytes were then negatively enriched with the Mouse CD8 T Lymphocyte Enrichment Set (BD Biosciences) and activated at $1x10^6$ cells per 24 well for 48 h with 2 μg/ml Concanavalin A (Merck) in RPMI 1640 supplemented with 8% FCS, penicillin/streptomycin, 50 μM β-mercapto-ethanol (Gibco), 10 ng/mL IL-2 (Immunotools), 0.5 ng/mL IL-7 (Immunotools) and 1 ng/mL IL-15 (Immunotools). After 48 h, cells were spun down and taken up in fresh medium at a concentration $1x10^6$ cells/ml. Cells were kept at a concentration of $1x10^6$/mL, with refreshment of media every 24 h, for 2–5 days before adoptive transfer.

In vitro cytokine stimulation

Ag^-CFP^+ tumor cells were plated at 200,000 cells per well in 6-well plates for 24 h and were then treated with either human IFNγ (Invitrogen), human TNFα (Peprotech), murine IFNγ (Thermo Fisher), murine TNFα (Peprotech) or murine TGFβ (ebioscience) the indicated combination, or were treated with culture medium from T cell - tumor cell co-cultures (see below), at the indicated concentrations or dilutions. At the indicated times, cells were harvested and used for bulk or single-cell RNA-seq, as indicated. For bulk RNA-seq, cells were lysed in RLT lysis buffer (Qiagen) and stored at −80°C before sequencing. The bulk RNA-seq datasets obtained from these *in vitro* cytokine-stimulated cells at different time points are referred to as the "OVCAR5 bulk RNA-seq reference dataset" and "NMM bulk RNA-seq reference dataset" throughout the manuscript. For single-cell RNA-seq, cells were stained with TotalSeq Hashtag antibodies (TotalSeq-B, Biolegend) and pooled, using an equal number of cells from each sample, to form one pool of cells for single cell RNA-seq analysis. Cell death and total cell counts were analyzed at 16 h or 44 h after treatment by IR-Dye staining and subsequent flow cytometry using AccuCountBlank 15.2-μm beads (Spherotech). To obtain culture medium from T cell - tumor cell co-cultures, Ag^+ GFP^+ OVCAR5 tumor cells were plated at $2x10^6$ per 10 cm culture dish. After 1 day, $4x10^6$ $CDK4_{R>L}$-specific $CD8^+$ T cells were added, and culture medium was harvested after 24 h, filtered through a 0.45 μm filter (GE) and stored at −80°C.

In vivo tumor models

$8x10^6$ OVCAR5 cells or $2x10^5$ NMM cells were injected subcutaneously into the flank of NSG-$\beta2m^{-/-}$ mice or C57BL/6; $RAG2^{-/-}$ mice, respectively, in 50 μL PBS (Gibco) and 50 μL matrigel (Corning), using the indicated mixtures of tumor cell variants. At day 7–8 after tumor inoculation, tumor-bearing mice received an intravenous injection of either 100 μL PBS or 5×10^6 $CDK4_{R>L}$ TCR-transduced $CD8^+$ T cells or GFP^+ OT-1 $CD8^+$ T cells in 100 μL PBS, as indicated. On days 0, 1 and 2 after T cell transfer, NSG-$\beta2m^{-/-}$ mice received injections of 7.2×10^5 IU IL-2 (Proleukin, Novartis) dissolved in 200 μL PBS, twice daily, with an interval of 6–12 h between injections, to support T cell engraftment. At the indicated times after T cell transfer, mice were sacrificed and tumors were harvested. Harvested tumors were manually minced and enzymatically digested in RPMI medium (Gibco) supplemented with 5 Wünsch units/ml TH Liberase/ml (Roche) 25 μg/mL DNase I (Roche) for 20 min at 37 °C under continuous shaking. Subsequently, cell digests were filtered through a 70-μm strainer (Falcon) and single-cell suspensions were stained with IR-Dye (Invitrogen) and TotalSeq Hastag antibodies (TotalSeq-A or B, Biolegend). Cells from each sample were combined at equal numbers, and CFP^+

(i.e., bystander) tumor cells were sorted from this cell pool on a FACSaria Fusion (BD biosciences) and analyzed by single-cell RNA-seq (see below). To measure cytokine production of intratumoral T cells *ex vivo*, tumor cells from digested tumors were subsequently cultured *in vitro* in the presence of Ag^- CFP^+ tumor cells (for digests from control tumors) or $CDK4_{R>L}$ Ag^+ tumor cells (for digests from Ag^+/Ag^- mixed tumors) for 3 h in the presence of Golgi-plug (BD biosciences) to block cytokine secretion. Cells were subsequently stained for intracellular IFNγ and TNFα and analyzed by flow cytometry.

Intratumoral cytokine injection

Where indicated, tumors of ~150 mm^3 size were intratumorally injected with 15ul PBS containing the indicated cytokines (100 ng IFNγ, 10 ng TNFα or 100 ng IFNγ *plus* 10 ng TNFα per mL of tumor mass), using a Veo insulin syringe with a BD Ultra-Fine 6 mm x 31G needle (BD biosciences). At the indicated times after injection, tumors were harvested, digested, sorted, and bystander tumor cells were analyzed by single-cell RNA-seq as described below.

Flow cytometry

For analysis of immune infiltrates in NSG-$\beta2m^{-/-}$ mice, cells were stained with fluorochrome-labeled anti-human CD3 antibody (clone OKT3; BD biosciences) in FACS buffer (PBS supplemented with 0.5% w/v bovine serum albumin (Sigma) and EDTA (2 mM, Life Technologies)) for 20–30 min at 4°C, while protected from light. For analysis of cytokine secretion of intratumoral T cells, cells were stained for anti-human CD3 (clone OKT3; BD biosciences), anti-mouse TCRβ constant domain (clone H57-597; BD Biosciences), anti-human IFNγ (clone 4S.B3; BD Biosciences) and anti-human TNFα (clone MAb11, eBioscience). After incubation, cells were washed twice with FACS buffer before resuspension in FACS buffer for analysis. IR-Dye (Invitrogen) was used to allow for live cell selection.

Bulk mRNA sequencing

Total RNA was isolated using the RNeasy Mini Kit (74106, Qiagen), including an on-column DNase digestion (79254, Qiagen), according to the manufacturer's instructions. RNA quality and quantity was assessed on the 2100 Bioanalyzer instrument, following the manufacturer's instructions "Agilent RNA 6000 Nano" (G2938-90034, Agilent Technologies). Total RNA samples having RIN values > 8 were subjected to TruSeq stranded mRNA library preparation, according to the manufacturer's instructions (Document # 1000000040498, Illumina). Stranded mRNA libraries were analyzed on a 2100 Bioanalyzer instrument, following the manufacturer's protocol "Agilent DNA 7500 kit" (G2938-90024, Agilent Technologies), diluted to 10 nM and pooled equimolar into multiplex sequencing pools for sequencing on HiSeq 2500 and NovaSeq 6000 instruments (Illumina). HiSeq 2500 single-end sequencing was performed using 65 cycles for Read 1, and 10 cycles for Read i7, using HiSeq SR Cluster Kit v4 cBot (GD-401-4001, Illumina) and HiSeq SBS Kit V4 50 cycle kit (FC-401-4002, Illumina). NovaSeq 6000 paired-end sequencing was performed using 54 cycles for Read 1, 19 cycles for Read i7, 10 cycles for Read i5, and 54 cycles for Read 2, using the NovaSeq 6000 SP Reagent Kit v1.5 (100 cycles) (20028401, Illumina).

Single cell gene expression library generation and sequencing

Single cell suspensions were diluted to a final concentration of 1,000 cells/μl in 1xPBS containing 0.04% weight/volume BSA. The Chromium Controller platform of 10X Genomics was used for single cell partitioning and barcoding. Per single cell suspension, each cell's transcriptome was barcoded during reverse transcription, pooled cDNA was amplified and Single Cell 3′ Gene Expression libraries and Cell Hashing libraries via Feature barcode technology were prepared, according to the manufacturer's protocol (CG000183, CG000206 and CG000317, 10X Genomics). All libraries were quantified on a 2100 Bioanalyzer Instrument following the Agilent Technologies Protocol (Agilent DNA 7500 kit, G2938-90024). Sequence library pools were composed and quantified by qPCR, according to the KAPA Library Quantification Kit Illumina Platforms protocol (KR0405, KAPA Biosystems). HiSeq 2500, NextSeq 550 or NovaSeq 6000 Illumina sequencing systems were used for paired-end sequencing of the Single Cell 3′ Gene Expression libraries and Cell Hashing libraries, respectively, at a sequencing depth of between 20,000–60,000 reads/cell and approximately 3,500 reads/cell. HiSeq 2500 paired-end sequencing was performed using 100 cycles for Read 1, 8 cycles for Read i7, and 100 cycles for Read 2, using HiSeq PE Cluster Kit V4 (PE-401-4001, Illumina) and multiple HiSeq SBS Kit V4 50 cycle kits (FC-401-4002, Illumina). NextSeq 550 paired-end sequencing was performed using 28 cycles for Read 1, 10 cycles for Read i7, and 54 cycles for Read 2, using the NextSeq 500/550 High Output Kit v2.5 (75 Cycles) (20024906, Illumina) and NextSeq 500/550 Mid Output Kit v2.5 (150 Cycles) (20024904, Illumina). Novaseq 6000 paired-end sequencing was performed using 28 cycles for Read 1, 10 cycles for each Read i7 and i5, and 90 cycles for Read 2, using the NovaSeq 6000 S2 Reagent Kit v1.5 (100 cycles) (20028316, Illumina). Gene expression and antibody sequencing reads were mapped to the GRCh38 human reference genome (refdata-cellranger-GRCh38–3.0.0) and antibody reference sequences, respectively, using CellRanger Version 5.0.1 in multi mode (10x Genomics) with default parameters. The genomic sequence of the Katushka fluorescent protein (named as ENSG00000555555) was added to the human reference prior to mapping.

Bulk RNA-seq data preprocessing

Bulk raw read counts of human OVCAR5 samples were mapped to CellRanger's reference transcriptome refdata-cellranger-GRCh38–3.0.0 using version 0.9 of the Nextflow core kallisto pipeline with kallisto 0.46.2. Read count distributions were *a priori* assessed using an awk script (as adapted from https://www.biostars.org/p/243552/). Transcript counts were collapsed to genes using

the R package tximport and Ensembl gene identifiers (IDs) were converted to HUGO gene names using a self-made lookup table generated from the CellRanger gtf file. Gene read counts were loaded into the R Seurat package, then TMM-library size normalized using edgeR and finally additionally corrected using Seurat's regularized negative binomial model regression, in the same manner as the single cell data (SCT normalization[44]). The last step had the effect of setting lowly expressed genes (fewer than 1 unit of TMM-normalized gene expression) to zero and also reduced the contrast in expression between highly and lowly expressed genes. Bulk sequencing data of murine NMM samples were aligned paired-end, strand and transcriptome aware, with hisat2[45] against GRCm38. Counts per gene were made using itreecount (https://github.com/NKI-GCF/itreecount) and annotated using ensembl gtf version 87.

Selection of cytokine-responsive genes

To identify cytokine-responsive genes for the OVCAR5 cell line using machine learning, we first devised a set of gene-characterizing features. A limma voom model[46] of the form $y \sim X_c\beta_c + X_d\beta_d$, where y reflects per gene expression levels, *X*s are design matrices, *c* reflect stimulus nature and concentration (one term for each combination of a tested stimulus and concentration), and *d* reflects stimulus exposure duration, was fitted to the 'OVCAR5 bulk RNA-seq reference dataset' described in the section '*in vitro cytokine stimulation*' and Figure 1. Duration coefficients were included to absorb confounding duration gene expression dynamics that were independent of the nature of stimulus. Interaction terms between stimuli and durations were not included as the design matrices would not be full-rank, as we had exactly one replicate per experimental condition. We collected the following statistics.

(1) Maximum *t*-statistics and effect sizes for the β_c terms were extracted from the fitted limma object.
(2) A cytokine specificity score, capturing the relative response to either TNFα or IFNγ, which was computed as $|\beta_{TNF\alpha}|/(|\beta_{TNF\alpha}|+|\beta_{IFN\gamma}|)$, where indicated coefficients reflect those of the highest tested concentrations of indicated cytokines (10 ng/mL for TNFα and 100 ng/mL for IFNγ). We have not noticed any genes responding more strongly to lower concentrations of a given stimulus, justifying this approach.
(3) A set of genes responded more strongly to the combination of IFNγ and TNFα than expected based on their response to these stimuli in isolation. To describe this synergistic behavior, a combined TNFα *plus* IFNγ synergy gene set score was computed as $\beta_{IFN\gamma+TNF\alpha}/(\beta_{TNF\alpha}+\beta_{IFN\gamma})$-1, where indicated coefficients again reflect the highest tested concentrations.
(4) As some genes responded very strongly to stimuli but only at specific timepoints and such effects would get diluted in the aforementioned limma model (which can be interpreted as an estimated average effect of concentration across the different tested exposure durations), single time point statistics were additionally extracted. For each stimulus and time point, the log2 fold difference with the duration-matched unstimulated control sample was computed, resulting in 3 additional statistics (IFNγ, TNFα and IFNγ *plus* TNFα), as well as the maximum of these three statistics.
(5) Genes for which one stimulus was consistently higher across the four tested timepoints appeared more informative than genes for which this was more variable. To describe this, the maximum number of exposure durations for which any given cytokine and concentration yielded the highest or lowest response was evaluated, yielding another two integral statistics ranging between 1 and 4.
(6) With the same goal in mind, the Pearson correlation between all three pairs of consecutive timepoints (2 & 6, 6 & 12, 12 & 24) across the different stimuli was recorded and summarized by the median across the three different sets. High-scoring genes on this metric will have high similarity in the ordering of stimuli in terms of effectuated gene expression across exposure durations. Line plots (as in Figure S2C) of such genes will appear ordered, i.e., with a low degree of line crossing.
(7) The maximum (log2-transformed) gene expression for each gene in the TMM-normalized expression data across samples was extracted, as well as the difference between the maximum and minimum gene expression values across samples.

The above features were computed for all 33,514 detected genes. As simple thresholding using these statistics gave suboptimal results (data not shown), the set of gene classifications was augmented from an original manually classified set of genes (n = 80) in an iterative process of i) random forest model fitting on already classified genes, with gene class as the response variable and the aforementioned features as explanatory variables ii) class prediction for previously unclassified genes and iii) manual curation of these model predictions (Figure S2A). For step i), classification random forests were trained using the ranger engine in R the tidymodels library with importance set to 'impurity', using the aforementioned gene descriptive statistics. The mtry parameter was optimized using 3-fold cross validation on a random, unique sample of 75% of the already classified genes, leaving 25% of the genes for validation purposes. A final model was trained on all the training data using optimal hyperparameters. The model was trained to discern between the following gene classes: 'cytokine-unresponsive' (a gene for which none of the evaluated exposures leads to clearly elevated gene expression as judged by inspection of line-plot as in Figure S2C) and 'cytokine-responsive' (responsive to at least one cytokine stimulus). The latter class was then subdivided into the following classes: 'mono-responsive (a cytokine-responsive gene responding strongly to one of the two tested cytokines but not to the other, and for which the combination of TNFα *plus* IFNγ does not behave differently from the dominant cytokine), 'synergistically-responsive' (a cytokine-responsive gene responding *solely* to the combination of TNFα *plus* IFNγ and not to the individual cytokines), 'other synergy' (a cytokine-responsive gene that shows a moderate degree of stimulus synergy but for which individual cytokines also effectuate noticeable gene expression), 'anti-synergy' (a cytokine-responsive gene whose response to the combination of stimuli is weaker than to the sum of the individual stimuli), 'lowly expressed' (possibly too lowly expressed to be reliably detectable in single cell data) and 'cytokine-responsive, other' (responsive to cytokine exposure, but not fitting to any of the aforementioned class descriptions). Step ii) the final model was used to

predict classes for all previously unclassified genes. Step iii) all 'cytokine-responsive' genes (and some 'cytokine-unresponsive' genes as well, to ensure the absence of false negative predictions) were inspected and predictions were adjusted where needed. After 10 iterations of model training and prediction curation, 612 cytokine-responsive genes were acquired (Figure S2D), at which point the yield of informative additional genes per additional cycle had slowed down to just a handful, suggesting nearly full extraction of all cytokine-responsive genes. For the purposes of this study, in which the 'other synergy', 'anti-synergy' and 'lowly expressed' classes are superfluous, genes belonging to these classes were next reclassified as 'cytokine-responsive, other' (Figure S2B). In addition, the 'mono-responsive' class was partitioned into 'IFNγ mono-responsive' (genes with cytokine specificity score $\leq$ 0.5) and 'TNFα mono-responsive' (genes with cytokine specificity score >0.5). Additionally, the following 'time-informative' gene sets were compiled by manual sub-selection from all 612 cytokine-responsive genes: IFNγ late and TNFα late (cytokine-responsive genes with a most pronounced response at 12–24 h of stimulation), IFNγ plateau (IFNγ-responsive genes rising in expression until 6 h, after which they remain constant) and TNFα early (genes responding most pronounced at 2 h of stimulation). TNFα plateau, as well as IFNγ early, mono-responsive genes could not be identified.

For the selection of genes for the IFNγ and TNFα gene sets for the murine NMM cell line, genes were prioritized using a simplification of the analysis done on the human OVCAR5 data. An identical limma model was fitted to the MNN bulk RNA-seq reference dataset, a candidate gene list was generated based on the resulting moderated *t*-statistics and candidate genes were then manually filtered for cytokine-unresponsive genes by inspecting their 'line' plots (as in Figure 1A), resulting in a total of 134 mono-responsive genes. TGFβ-responsive genes in the Milo analysis (Figure 4E) were identified by filtering based on limma moderated *t*-statistics, with a limma model as described above applied resulting in one *t*-statistic for each of the evaluated single stimuli per gene. Genes were included if they were found mono-responsive to TGFβ, i.e., a) a *t*-statistic surpassing 4.2 for TGFβ and b) below 1 for all other evaluated single stimuli. Genes were then filtered for biological, as opposed to purely technical, expression variation using the modelGeneVar function in the R package scran, which was called with log2(cpm +1) transformed data and with exposure duration meta information as the function's argument to 'block'. Genes were required to have bio >0 and FDR $\leq$ 10^-7, resulting in a total of 73 TGFβ mono-responsive genes.

Human ovarian carcinoma single cell sequencing data preprocessing

CellRanger UMI count data was loaded into R Seurat objects and cells with less than 1,000 detected RNA features were filtered out. Across single cell sequencing experiments, either a single or two hashtag bar codes per sample (i.e., experimental condition) were employed, the latter to allow inclusion of a larger number of samples than the number of available hashtagging antibodies. Sample assignment for experiments employing single hashtagging was done using Seurat's HTODemux functionality on the CLR-normalized barcode hashtag data using default settings. Sample assignment for experiments employing double hashtagging was done using a custom functionality. First, HTOs were CLR normalized using Seurat's NormalizeData. Next, the product of normalized hashtag counts was computed for each theoretically possible combination of two different hashtag antibodies. Cells were assigned to the sample corresponding to the highest product of CLR-normalized hashtag counts. Low-confidence assignments were then filtered out based on the fold difference between the dominant and second to dominant hashtag combination. A threshold value of 2 for this statistic was picked by comparing cells for which the dominant combination of hashtags was expected (i.e., a combination included in the experimental design) and those for which it was not. Cells were additionally filtered for a maximum mitochondrial content of 30%. SCT total UMI count normalization was performed on the remaining set of cells.[44] We next identified the most variable features in the experiment (Seurat's FindVariableFeatures with default settings) and performed principal component analysis with 10 principal components (sufficient, as indicated by scree plots, obtained using Seurat's RunPCA, default settings) and a UMAP (Seurat's RunUMAP, default settings) over the principal component scores. Next, outlying clusters in the UMAP were automatically identified using density-based clustering on the UMAP cell coordinates with DBSCAN (fpc package) using parameters: eps = 0.6 and MinPts = 6. Small DBSCAN clusters (less than 1/(5*c*) cells, where c is the number of detected DBSCAN clusters) were then marked as outlying clusters and removed from downstream analyses. Using differential gene expression analysis (Seurat's FindMarkers) and GSEA with (R 'fgsea' package) with REACTOME pathways[47] on the logFC-ranked list of differentially expressed genes (filtered first FDR-adjusted p value $\leq$ 0.1) between the outlying cluster and the main body of cells (i.e., the composite of non-outlying clusters), we identified these outlying clusters (0%–2.7% of cells across experiments) to likely consist of keratinocytes and/or fibroblasts, characterized by high *KRT81, S100A9* and *LDHB* counts. SCT normalization was redone on the remaining cells. Using the intersection of cytokine-responsive genes and detectable genes for each experiment, PCA was recomputed with 10 PCs and UMAPs were recomputed based on the PC scores.

Murine NRAS mutant melanoma single cell sequencing data preprocessing

The murine NMM data were preprocessed identically to the human OVCAR5 single cell data. Inspecting the initial UMAP, we noticed two clusters of cells. Characterizing the smaller cluster (DBSCAN cluster 2, 21.5% of cells), we noticed a 7.2-fold difference in mean UMIs between clusters (47,753 versus 6,654 mean UMI), suggestive of the presence of dying cells and/or cell fragments in the second cluster. Cells in this cluster were then removed, and SCT normalization, PCA and UMAP computation was repeated on the remaining cells.

Heatmap visualization of bulk RNA-seq data

TMM and SCT normalized data were log2-transformed and subsequently Z-scaled across genes/features. Unless indicated otherwise, rows (genes) and columns (samples) were subsequently clustered using complete linkage hierarchical clustering (hclust function in R), using Spearman correlation distance (computed as $1 - c$, where c is the correlation between two samples) for genes (rows) and Euclidean distance for samples (columns).

Gene set scores for single cell data

For both OVCAR5 and NMM cell lines, gene set scores were computed by summing SCT-normalized expression values of a gene set's member genes. Where indicated, gene set scores were normalized to the distribution of gene set scores of a relevant, duration-matched control condition with the following transformation: $f(x)=(x-m(x_c))/IQR(x_c)$, where m represents the median, x_c is a vector of scores for the same gene set for a reference condition and $IQR(x_c)$ is the interquartile range in that reference population.

Quantification of separability of experimental conditions using gene set scores

To distinguish more than two classes at a time, as in Figure 2B, we trained SVM models using the Gaussian kernel on 75% of the data, leaving the remaining 25% as validation data, with the R tidymodels framework. Hyperparameters cost and rbf_sigma were optimized in a 10-fold cross validation within the training data. Optimal parameters were then used to train a final model on the full set of training data, of which the performance was subsequently evaluated on the validation data. Included confusion matrices show the correspondence between actual and predicted class labels in the validation data, using a model trained on independent data, ignoring the fact that single cell transcriptomes in the training and validation sets were jointly preprocessed.

Milo neighborhood analysis of single cell data

A PCA of the murine single cell data was computed using the 2,000 most variable genes (as identified using Seurat's FindVariableGenes with default settings) and 20 principal components. A KNN graph of the data was constructed on the principal component scores with Milo's buildGraph function using k = 10 and d = 20. Neighborhoods were defined using makeNhoods, with refined = TRUE, prop = 0.1 and identical settings for k and d as aforementioned. Neighborhoods were tested for differential abundance of the three experimental conditions using the testNhoods function, with a design matrix that was obtained from a metadata table with the following R model formula: ~1 + experimental condition, resulting in an intercept term and a regression coefficient for the second and third experimental conditions. In visualizations of the KNN graph, effect sizes (logFC DA) associated with a Spatial FDR >0.05 were whitened.

Deconvolution analysis of single cell neighborhood expression

A gene expression matrix of g genes (rows) by n single cell neighborhoods (SCNs, columns) in linear space was extracted using the Milo nhoodExpression class method, TMM-transformed to normalize library sizes and finally log10-transformed, i.e., $M_N = log\ 10(TMM(X) + 1)$, wherein X is the output of nhoodExpression and M_N is the processed matrix of SCN expression. Similarly, a g x 28 reference profile matrix M_R consisting of bulk reference RNA-seq libraries with the 28 conditions/columns unstimulated 2 h - unstimulated 24h (i.e., no stimulation for 2 h followed by no stimulation for another 24 h), unstimulated 2 h - 10 ng/mL TGFb 24 h, unstimulated 2 h - 100 ng/mL IFNy 24 h, 10 ng/mL TGFb 2 h - unstimulated 24 h, 10 ng/mL TGFb 2 h - 100 ng/mL IFNy 24 h, 100 ng/mL IFNy 2 h - unstimulated 24 h, 100 ng/mL IFNy 2 h - 10 ng/mL TGFb 24 h, unstimulated 6 h - unstimulated 24 h, unstimulated 6 h - 10 ng/mL TGFb 24 h, unstimulated 6 h - 100 ng/mL IFNy 24 h, 10 ng/mL TGFb 6 h - unstimulated 24 h, 10 ng/mL TGFb 6 h - 100 ng/mL IFNy 24 h, 100 ng/mL IFNy 6 h - unstimulated 24 h, 100 ng/mL IFNy 6 h - 10 ng/mL TGFb 24 h, unstimulated 12 h - unstimulated 24 h, unstimulated 12 h - 10 ng/mL TGFb 24 h, unstimulated 12 h - 100 ng/mL IFNy 24 h, 10 ng/mL TGFb 12 h - unstimulated 24 h, 10 ng/mL TGFb 12 h - 100 ng/mL IFNy 24 h, 100 ng/mL IFNy 12 h - unstimulated 24 h, 100 ng/mL IFNy 12 h - 10 ng/mL TGFb 24 h, unstimulated 24 h - unstimulated 24 h, unstimulated 24 h - 10 ng/mL TGFb 24 h, unstimulated 24 h - 100 ng/mL IFNy 24 h, unstimulated 24 h - 100 ng/mL IFNy 10 ng/mL TGFb 24 h, 10 ng/mL TGFb 24 h - unstimulated 24 h, 10 ng/mL TGFb 24 h - 100 ng/mL IFNy 24 h, 100 ng/mL IFNy 24 h - unstimulated 24 h, 100 ng/mL IFNy 24 h - 10 ng/mL TGFb 24 h in the columns and genes in the rows) were TMM-normalized and then similarly log10-transformed. The matrices were identically row-ordered (genes), with as rows the intersection of detected genes in the two unprocessed source matrices ($g = 14,620$) such that they predominantly consisted of genes that are minimally or not responsive to the cytokines of interest.

To estimate an SCN's stimulus exposure, its transcriptome was modeled as a linear combination of the columns (samples) of M_R using lasso $l1$-penalized multivariate regression with the regression coefficients (β) constrained to be larger than or equal to 0, such that they can be interpreted as mixing weights. The cv.glmnet function from the R package glmnet was used for this regression,[48] as well as to optimize the lambda penalty for regression coefficients with arguments: lower.limits = c(0), family = 'Gaussian', alpha = 0.99. The mean squared error between the original transcriptome (y) and reconstructed transcriptome ($x\ \beta$), i.e.,. $E[(y - x\ \beta)^2]$, was then extracted from the cv.glmnet object with `lambda` set to the value that minimized the cross validation error. To assess the importance of a subset of reference samples (columns) c for the reconstruction of any particular SCN, the reconstruction error was recomputed with the remaining columns of M_R after having removed samples/columns c. In this, a large increase in error can be interpreted as an indication that the samples c contain co-variation in gene expression that cannot be accommodated by any of the remaining reference samples. To quantify the possibility that reconstruction error was simply raised by providing the optimization algorithm a smaller set of basis vectors to work with (i.e., by limiting the span of M_R), permutation testing was employed. Specifically,

the reconstruction error was first computed with 1,000 random selections of *s* reference profiles, where *s* is the number of reference profiles that were *not* associated with the reference profiles (columns) of which the importance is assessed. For example, to assess the importance of TGFβ stimulation, *s* is the number of profiles obtained from experiments where no TGFβ stimulation was applied (i.e., only unstimulated and IFNγ stimulated samples, $s = 11$, Figure 4G, left). Similarly, to assess the importance of IFNγ stimulation, *s* represents the number of profiles obtained from experiments where no IFNγ stimulation was applied (i.e., only unstimulated and TGFβ-stimulated samples, $s = 11$, Figure 4G, right). The quantile of the observed error in the distribution of permutation errors was then acquired using the R function ecdf. SCN reconstruction was finally labeled as worse (or better) than expected if the observed error was in the 97.5st or higher (or 2.5 th or lower) percentile of the permutation distribution.

QUANTIFICATION AND STATISTICAL ANALYSIS

Statistical analyses for flow cytometry data were performed in Prism (GraphPad). Statistical details for experiments, including the statistical test used, the value of *n*, what *n* represents, and the obtained p values can be found in the figure and/or figure legends. No statistical method was used to predetermine sample sizes. No data were excluded from the analyses.

AUROC values used for single cell RNA-seq data in the main text and figures represent the area under the receiver operator curve from a binary classifier aiming to separate the two indicated experimental conditions with the indicated gene set score as the sole explanatory variable. These scores were computed using the roc_auc_vec function in the R yardstick package. AUROC values range between 0.5 (signifying no separation between experimental conditions) and 1 (signifying complete separation between experimental conditions).